experiment, periostin ΔbΔe continuously activated the phosphorylation of FAK for 9 h after the addition of it to serum-starved cell cultures, whereas in the control, the signal had decreased by 6 h (Fig. 4 D). These results demonstrate that periostin ΔbΔe activated FAK phosphorylation and promoted formation of dynamic protrusions. Next, we tested the motility of primary cardiac fibroblasts from *periostin*$^{-/-}$ mice in the presence of periostin ΔbΔe. The result showed that periostin ΔbΔe strongly activated the cell migration of these fibroblasts (Fig. 4 E). Moreover, this migration caused by periostin ΔbΔe was significantly reduced by antibodies against either periostin or αv-integrin; by PP2, which is known as a compound that specifically inhibits adhesion-induced FAK phosphorylation (28); and by knockdown of FAK by siRNA (Fig. 4 E), suggesting that periostin ΔbΔe would activate the cell motility of their fibroblasts by FAK signaling through αv-integrin in mice subjected to AMI. Finally, we inhibited the integrin-mediated FAK pathway by using chemical compounds and siRNAs (Fig. 4 F). FAK inhibitors or siRNA down-regulated the Akt phosphorylation, and Akt inhibitors did not change FAK phosphorylation after stimulation by periostin ΔbΔe, indicating that Akt is a downstream molecule of FAK and periostin ΔbΔe. Moreover, αv-integrin siRNA treatment blocked both FAK and Akt phosphorylation after stimulation by periostin ΔbΔe. These results indicate that periostin ΔbΔe can stimulate FAK and Akt phosphorylation through αv-integrin.

We demonstrated that in the case of periostin deficiency, the collagen amount was reduced in the infarct myocardium, resulting in frequent cardiac rupture in the AMI. Our results, together with the previous findings by Norris et al. (7) on the role of periostin in collagen fibrillogenesis of skin and tendon, strongly suggest that fibrillar collagen formation, which contributes essentially to a mechanically stable scar formation, was impaired in the early stage of MI in the periostin deficiency, resulting in a high rate of cardiac rupture. Furthermore, we have found that the reduced mechanical strength, rupture of the infarct region, and repression of LV dilation in periostin deficiency were most likely caused by a reduced number of cardiac fibroblasts and by the insufficient creation of a durable collagen network caused by a lower rate of collagen synthesis and cross-linking. To reveal more about the importance of collagen production or collagen cross-linking for protection against heart rupture, after AMI, we treated mice with an inhibitor of lysyl oxidase, thus inhibiting collagen cross-linking. Interestingly, the data showed a high amount of collagen production with a larger number of vimentin-positive cells in the infarct region, resulting in effective blockage of heart rupture (unpublished data). These data suggest that periostin-stimulated migration of cardiac fibroblasts into the infarct region, the cells of which produce a high amount of collagen, is more essential than collagen cross-linking by periostin.

The expression of TGFβ was markedly up-regulated in the infarct border during the scar formation phase after AMI, and the phosphorylation of smad 2/3 was consequently increased (unpublished data), whereas there was no significant difference in the TGFβ transcription level between *periostin*$^{+/+}$ and $^{-/-}$ mice; TGFβ also enhanced the periostin expression in the infarct border after AMI because anti-TGFβ antibody treatment blocked the periostin expression (Fig. S6, available at http://www.jem.org/cgi/content/full/jem.20071297/DC1). The expression of both TGFβ and periostin is up-regulated by angiotensin II and attenuated by angiotensin receptor blockers after AMI (29, 30), suggesting that periostin may play a role via angiotensin II-TGFβ signaling. The combined results on the biomechanical properties and the collagen content of the isolated infarct heart support the concept that the periostin-linked collagen fibrous skeleton is an important determinant of cardiac rupture.

The results given here indicate that periostin signals activate cell migration of cardiac fibroblasts from outside into the infarct region through FAK phosphorylation, and then the migrated cells differentiate into αSMA-positive fibroblasts, resulting in strengthening of the stiffness of the LV wall through collagen synthesis after AMI. FAK is known to be involved in tyrosine phosphorylation during integrin-mediated signaling, and this molecule plays an important role in the response of migrating cells to mechanical stress (31). Recently, FAK has been implicated as a downstream target associated with angiotensin II–stimulated cell migration (32). The mechanism underlying the periostin action of promoting the recruitment of cardiac fibroblasts followed by healing of the infarct region appears to involve activation of the FAK pathway, indicating that the periostin-induced increase in FAK phosphorylation in the infarct myocardium enhanced the motility of these fibroblasts. In contrast, three-dimensional culture studies imply that the matrix stiffness regulates cell fate by modulating integrin signaling (31, 33). Considering these accumulated results, we suggest that periostin is mainly produced by fibroblasts through angiotensin II–TGFβ signaling and may convey pathologically rapid reinforced mechanical signals to FAK-integrin signaling after AMI. The fibroblastic cells activated by these signals secrete periostin, which in turn increases their motility, contractility, and synthesis of ECM proteins, thus promoting further recruitment and activation of fibroblasts. Periostin may serve as the trigger of these feedback mechanisms in the ongoing healing processes. Additional studies to elucidate in more detail the characteristics of cardiac fibroblasts may lead to a deeper understanding of the role of periostin after AMI, as well as aid in identifying the molecular targets of therapies to augment cardiac performance and wall stiffness after AMI.

MATERIALS AND METHODS

Preparation of rabbit polyclonal antibodies against periostin. We raised polyclonal RD1 antibodies against periostin by using the peptide DNLDSDIRRGLESNVN (representing aa 143–158 of human periostin) for human periostin and the peptide ENLDSDIRRGLENNVN (representing aa 145–160 of mouse periostin) for mouse periostin. The antibodies were affinity-purified by using the respective immunogenic peptide.

Histology, immunostaining, and electron microscopy. Human tissue samples were obtained during autopsy and fixed in 4% neutral formalin or 20% formalin. A total of 41 cases, ranging from a fetus to an 89-yr-old patient, including 15 cases of myocardial infarction, were examined. All the cases were approved for use in research by the Ethics Committee of the

University of Tokyo. After having been embedded in paraffin, specimens were cut at a 4-μm thickness. Hematoxylin and eosin, elastica von Gieson, and Azan staining procedures were performed. Immunohistochemistry by the ABC method was done by using an i6000 apparatus (Biogenex).

For histological analysis of the infarcted mice, the animals were killed at 1, 2, 3, 4, 5, 7, 14, or 28 d after surgery under anesthesia, and were perfusion fixed with 4% paraformaldehyde at physiological pressure. Fixed hearts were sectioned transversely into three equal segments from their apex to base and cryoembedded or embedded in paraffin. 4-μm-thick sections were used for histological analysis or for immunostaining. Antibodies against αv-integrin (Laboratory Vision), αSMA (Sigma-Aldrich), FAK (BD Biosciences), pY397FAK (Invitrogen), pS473Akt (Cell Signaling Technology), Akt (Cell Signaling Technology), collagen I (Novotec), fibronectin (34), Ki67 (YLEM), active caspase3 (Promega), vimentin (PROGEN), smooth muscle myosin-1 (SM1; Kyowa Hakko Ltd.), and Mac3 (BD Biosciences) were used for immunostaining. Antigen unmasking techniques were not performed, except for anti–αv-integrin. For immunostaining of pY397FAK and pS473Akt, the Catalyzed Signal Amplification system was used (Dako). In the case of fluorescence studies, the signals were observed under a confocal microscope (FLUOVIEW FV1000; Olympus).

Sections of infarcted heart were generated from 6 *periostin*$^{+/+}$ and 6 $^{-/-}$ male mice at 5 and 28 d after AMI, and they were prepared for electron microscopy as previously described (35). Sham-operated mice were used for the control. Collagen fibril diameters were measured in scanned images generated from electron micrographs with Image J software. Collagen fibrils and the number of vimentin-positive or αSMA-positive cells in at least 6 fields derived from each of the basement-, mid-, and apex-part of the infarct region of heart sections were quantified (6 mice per group). Animal studies were conducted under a protocol approved by the Institutional Animal Use and Care Committee.

Quantification of collagen cross-links and collagen contents. Snap-frozen infarct tissues from *periostin*$^{+/+}$ and $^{-/-}$ mice were used. Pyridinoline and hydroxyproline contents were determined by the previously described HPLC method (36).

Adenovirus-mediated gene transfer. Construction of Ad-nlsLacZ and Ad-periostin ΔbΔe vectors was performed by use of an Adeno-X Expression System 2 (BD Biosciences). The virus purification method used, involving cesium chloride ultracentrifugation, was previously described (37). 1 d before LAD ligation, a volume of 100 μl containing 1.6×10^{10} PFU of Ad-nlsLacZ or Ad-periostin ΔbΔe virus was injected into a tail vein of male *periostin*$^{-/-}$ mice.

Statistical analysis. All numerical results were presented as the mean ± the SEM. Statistical analyses of the echocardiography and cell migration assay were performed with a Student's unpaired *t* test. Cardiac rupture frequency was compared by the χ^2 test. Survival curves after AMI were obtained by the Kaplan-Meier method, and compared by the log-rank test. Differences were considered significant at $P < 0.05$.

Online supplemental material. Fig. S1 shows the confirmation of the periostin expression in cardiac fibroblasts. Fig. S2 indicates the generation of *periostin*$^{-/-}$ mice. Fig. S3 shows the immunofluorescence analysis of fibronectin after AMI. Fig. S4 shows immunofluorescence analysis for gene-transferred *periostin*$^{-/-}$ infarct heart. Fig. S5 depicts the analysis for the phosphorylation of Akt after AMI. Fig. S6 shows a cause-and-effect relationship between TGFβ and periostin after AMI. Table S1 provides the echocardiographic data. Full methods and associated references are available in the Supplemental materials and methods. The online version of this article is available at http://www.jem.org/cgi/content/full/jem.20071297/DC1.

The authors thank M. Ikumi and E. Ikeno for technical assistance in generating knockout mice; S. Matsumura and M. Yoshioka for their technical help in the LV rupture threshold study; and S. Sakaguchi for her support, patience, and comprehension.

This research was supported by grants-in-aid from the Ministry of Education, Culture, Sports, Science, and Technology of Japan to A. Kudo and Y. Saga.

The authors have no conflicting financial interests.

Submitted: 25 June 2007
Accepted: 17 December 2007

REFERENCES

1. Horiuchi, K., N. Amizuka, S. Takeshita, H. Takamatsu, M. Katsuura, H. Ozawa, Y. Toyama, L.F. Bonewald, and A. Kudo. 1999. Identification and characterization of a novel protein, periostin, with restricted expression to periosteum and periodontal ligament and increased expression by transforming growth factor beta. *J. Bone Miner. Res.* 14:1239–1249.
2. Gillan, L., D. Matei, D.A. Fishman, C.S. Gerbin, B.Y. Karlan, and D.D. Chang. 2002. Periostin secreted by epithelial ovarian carcinoma is a ligand for alpha(V)beta(3) and alpha(V)beta(5) integrins and promotes cell motility. *Cancer Res.* 62:5358–5364.
3. Bao, S., G. Ouyang, X. Bai, Z. Huang, C. Ma, M. Liu, R. Shao, R.M. Anderson, J.N. Rich, and X.F. Wang. 2004. Periostin potently promotes metastatic growth of colon cancer by augmenting cell survival via the Akt/PKB pathway. *Cancer Cell.* 5:329–339.
4. Lindner, V., Q. Wang, B.A. Conley, R.E. Friesel, and C.P.H. Vary. 2005. Vascular injury induces expression of periostin: implications for vascular cell differentiation and migration. *Arterioscler. Thromb. Vasc. Biol.* 25:77–83.
5. Li, G., S. Oparil, J.M. Sanders, L. Zhang, M. Dai, L.B. Chen, S.J. Conway, C.A. McNamara, and I.J. Sarembock. 2006. Phosphatidylinositol-3-kinase signaling mediates vascular smooth muscle cell expression of periostin in vivo and in vitro. *Atherosclerosis.* 188:292–300.
6. Butcher, J.T., R.A. Norris, S. Hoffman, C.H. Mjaatvedt, and R.R. Markwald. 2007. Periostin promotes atrioventricular mesenchyme matrix invasion and remodeling mediated by integrin signaling through Rho/PI 3-kinase. *Dev. Biol.* 302:256–266.
7. Norris, R.A., B. Damon, V. Mironov, V. Kasyanov, A. Ramamurthi, R. Moreno-Rodriguez, T. Trusk, J.D. Potts, R.L. Goodwin, J. Davis, et al. 2007. Periostin regulates collagen fibrillogenesis and the biomechanical properties of connective tissues. *J. Cell. Biochem.* 101:695–711.
8. Kruzynska-Frejtag, A., M. Machnicki, R. Rogers, R.R. Markwald, and S.J. Conway. 2001. Periostin (an osteoblast-specific factor) is expressed within the embryonic mouse heart during valve formation. *Mech. Dev.* 103:183–188.
9. Stanton, L.W., L.J. Garrard, D. Damm, B.L. Garrick, A. Lam, A.M. Kapoun, Q. Zheng, A.A. Protter, G.F. Schreiner, and R.T. White. 2000. Altered patterns of gene expression in response to myocardial infarction. *Circ. Res.* 86:939–945.
10. Urasawa, K., I. Yoshida, C. Takagi, H. Onozuka, T. Mikami, H. Kawaguchi, and A. Kitabatake. 1996. Enhanced expression of beta-adrenergic receptor kinase 1 in the hearts of cardiomyopathic Syrian hamsters, BIO53.58. *Biochem. Biophys. Res. Commun.* 219:26–30.
11. Wang, D., S. Oparil, J.A. Feng, P. Li, G. Perry, L.B. Chen, M. Dai, S.W. John, and Y.F. Chen. 2003. Effects of pressure overload on extracellular matrix expression in the heart of the atrial natriuretic peptide-null mouse. *Hypertension.* 42:88–95.
12. Katsuragi, N., R. Morishita, N. Nakamura, T. Ochiai, Y. Taniyama, Y. Hasegawa, K. Kawashima, Y. Kaneda, T. Ogihara, and K. Sugimura. 2004. Periostin as a novel factor responsible for ventricular dilation. *Circulation.* 110:1806–1813.
13. Bujak, M., and N.G. Frangogiannis. 2007. The role of TGF-beta signaling in myocardial infarction and cardiac remodeling. *Cardiovasc. Res.* 74:184–195.
14. Sun, Y., and K.T. Weber. 2000. Infarct scar: a dynamic tissue. *Cardiovasc. Res.* 46:250–256.
15. Virag, J.I., and C.E. Murry. 2003. Myofibroblast and endothelial cell proliferation during murine myocardial infarct repair. *Am. J. Pathol.* 163:2433–2440.
16. Tomasek, J.J., G. Gabbiani, B. Hinz, C. Chaponnier, and R.A. Brown. 2002. Myofibroblasts and mechano-regulation of connective tissue remodelling. *Nat. Rev. Mol. Cell Biol.* 3:349–363.
17. Heymans, S., A. Luttun, D. Nuyens, G. Theilmeier, E. Creemers, L. Moons, G.D. Dyspersin, J.P.M. Cleutjens, M. Shipley, A. Angellilo,

et al. 1999. Inhibition of plasminogen activators or matrix metalloproteinases prevents cardiac rupture but impairs therapeutic angiogenesis and causes cardiac failure. *Nat. Med.* 5:1135–1142.

18. Matsumura, S.-I., S. Iwanaga, S. Mochizuki, H. Okamoto, S. Ogawa, and Y. Okada. 2005. Targeted deletion or pharmacological inhibition of MMP-2 prevents cardiac rupture after myocardial infarction in mice. *J. Clin. Invest.* 115:599–609.
19. Matsusaka, H., T. Ide, S. Matsushima, M. Ikeuchi, T. Kubota, K. Sunagawa, S. Kinugawa, and H. Tsutsui. 2006. Targeted deletion of p53 prevents cardiac rupture after myocardial infarction in mice. *Cardiovasc. Res.* 70:457–465.
20. Nahrendorf, M., K. Hu, S. Frantz, F.A. Jaffer, C.-H. Tung, K.-H. Hiller, S. Voll, P. Nordbeck, D. Sosnovik, S. Gattenlohner, et al. 2006. Factor XIII deficiency causes cardiac rupture, impairs wound healing, and aggravates cardiac remodeling in mice with myocardial infarction. *Circulation.* 113:1196–1202.
21. Askari, A.T., M.-L. Brennan, X. Zhou, J. Drinko, A. Morehead, J.D. Thomas, E.J. Topol, S.L. Hazen, and M.S. Penn. 2003. Myeloperoxidase and plasminogen activator inhibitor 1 play a central role in ventricular remodeling after myocardial infarction. *J. Exp. Med.* 197:615–624.
22. Sun, M., F. Dawood, W.-H. Wen, M. Chen, I. Dixon, L.A. Kirshenbaum, and P.P. Liu. 2004. Excessive tumor necrosis factor activation after infarction contributes to susceptibility of myocardial rupture and left ventricular dysfunction. *Circulation.* 110:3221–3228.
23. Ichihara, S., T. Senbonmatsu, E. Price Jr., T. Ichiki, F.A. Gaffney, and T. Inagami. 2002. Targeted deletion of angiotensin II type 2 receptor caused cardiac rupture after acute myocardial infarction. *Circulation.* 106:2244–2249.
24. Michael, L.H., M.L. Entman, C.J. Hartley, K.A. Youker, J. Zhu, S.R. Hall, H.K. Hawkins, K. Berens, and C.M. Ballantyne. 1995. Myocardial ischemia and reperfusion: a murine model. *Am. J. Physiol.* 269:H2147–H2154.
25. Lindsley, A., W. Li, J. Wang, N. Maeda, R. Rogers, and S.J. Conway. 2005. Comparison of the four mouse fasciclin-containing genes expression patterns during valvuloseptal morphogenesis. *Gene Expr. Patterns.* 5:593–600.
26. Stambolic, V., and J.R. Woodgett. 2006. Functional distinctions of protein kinase B/Akt isoforms defined by their influence on cell migration. *Trends Cell Biol.* 16:461–466.
27. Mitra, S.K., D.A. Hanson, and D.D. Schlaepfer. 2005. Focal adhesion kinase: in command and control of cell motility. *Nat. Rev. Mol. Cell Biol.* 6:56–68.
28. Hakuno, D., T. Takahashi, J. Lammerding, and R.T. Lee. 2005. Focal adhesion kinase signaling regulates cardiogenesis of embryonic stem cells. *J. Biol. Chem.* 280:39534–39544.
29. Iekushi, K., Y. Taniyama, J. Azuma, N. Katsuragi, N. Dosaka, F. Sanada, N. Koibuchi, K. Nagao, T. Ogihara, and R. Morishita. 2007. Novel mechanisms of valsartan on the treatment of acute myocardial infarction through inhibition of the antiadhesion molecule periostin. *Hypertension.* 49:1409–1414.
30. Berk, B.C., K. Fujiwara, and S. Lehoux. 2007. ECM remodeling in hypertensive heart disease. *J. Clin. Invest.* 117:568–575.
31. Wang, H.-B., M. Dembo, S.K. Hanks, and Y.-l. Wang. 2001. Focal adhesion kinase is involved in mechanosensing during fibroblast migration. *Proc. Natl. Acad. Sci. USA.* 98:11295–11300.
32. Baudino, T.A., W. Carver, W. Giles, and T.K. Borg. 2006. Cardiac fibroblasts: friend or foe? *Am. J. Physiol. Heart Circ. Physiol.* 291:H1015–H1026.
33. Bershadsky, A.D., N.Q. Balaban, and B. Geiger. 2003. Adhesion-dependent cell mechanosensitivity. *Annu. Rev. Cell Dev. Biol.* 19:677–695.
34. Arai, S., N. Amizuka, Y. Azuma, S. Takeshita, and A. Kudo. 2003. Osteoclastogenesis-related antigen, a novel molecule on mouse stromal cells, regulates osteoclastogenesis. *J. Bone Miner. Res.* 18:686–695.
35. Kii, I., N. Amizuka, L. Minqi, S. Kitajima, Y. Saga, and A. Kudo. 2006. Periostin is an extracellular matrix protein required for eruption of incisors in mice. *Biochem. Biophys. Res. Commun.* 342:766–772.
36. Saito, M., K. Marumo, K. Fujii, and N. Ishioka. 1997. Single-column high-performance liquid chromatographic-fluorescence detection of immature, mature, and senescent cross-links of collagen. *Anal. Biochem.* 253:26–32.
37. Ugai, H., T. Yamasaki, M. Hirose, K. Inabe, Y. Kujime, M. Terashima, B. Liu, H. Tang, M. Zhao, T. Murata, et al. 2005. Purification of infectious adenovirus in two hours by ultracentrifugation and tangential flow filtration. *Biochem. Biophys. Res. Commun.* 331:1053–1060.

Local Tenomodulin Absence, Angiogenesis, and Matrix Metalloproteinase Activation Are Associated With the Rupture of the Chordae Tendineae Cordis

Naritaka Kimura, MD; Chisa Shukunami, DDS, PhD; Daihiko Hakuno, MD, PhD; Masatoyo Yoshioka, MD, PhD; Shigenori Miura, PhD; Denitsa Docheva, PhD; Tokuhiro Kimura, MD; Yasunori Okada, MD, PhD; Goki Matsumura, MD, PhD; Toshiharu Shin'oka, MD, PhD; Ryohei Yozu, MD, PhD; Junjiro Kobayashi, MD, PhD; Hatsue Ishibashi-Ueda, MD, PhD; Yuji Hiraki, PhD; Keiichi Fukuda, MD, PhD

Background—Rupture of the chordae tendineae cordis (CTC) is a well-known cause of mitral regurgitation. Despite its importance, the mechanisms by which the CTC is protected and the cause of its rupture remain unknown. CTC is an avascular tissue. We investigated the molecular mechanisms underlying the avascularity of CTC and the correlation between avascularity and CTC rupture.

Methods and Results—We found that tenomodulin, which is a recently isolated antiangiogenic factor, was expressed abundantly in the elastin-rich subendothelial outer layer of normal rodent, porcine, canine, and human CTC. Conditioned medium from cultured CTC interstitial cells strongly inhibited tube formation and mobilization of endothelial cells; these effects were partially inhibited by small-interfering RNA against tenomodulin. The immunohistochemical analysis was performed on 12 normal and 16 ruptured CTC obtained from the autopsy or surgical specimen. Interestingly, tenomodulin was locally absent in the ruptured areas of CTC, where abnormal vessel formation, strong expression of vascular endothelial growth factor-A and matrix metalloproteinases, and infiltration of inflammatory cells were observed, but not in the normal or nonruptured area. In anesthetized open-chest dogs, the tenomodulin layer of tricuspid CTC was surgically filed, and immunohistological analysis was performed after several months. This intervention gradually caused angiogenesis and expression of vascular endothelial growth factor-A and matrix metalloproteinases in the core collagen layer in a time-dependent manner.

Conclusions—These findings provide evidence that tenomodulin is expressed universally in normal CTC in a concentric pattern and that local absence of tenomodulin, angiogenesis, and matrix metalloproteinase activation are associated with CTC rupture. (***Circulation.*** **2008;118:1737-1747.)**

Key Words: angiogenesis ■ chordae tendineae cordis ■ metalloproteinases ■ tenomodulin ■ valves

Although the heart is a vascularized organ, the cardiac valves and chordae tendineae cordis (CTC) are avascular tissues.[1] This avascularity is abrogated in several valvular heart diseases (VHDs).[2–4] Chondromodulin-I, which is an antiangiogenic factor isolated from bovine cartilage,[5–8] is also expressed in the eye and is critically involved in the maintenance. Recently, we have reported that chondromodulin-I was abundantly expressed by the valvular interstitial cells in normal cardiac valves.[9] Gene targeting of chondromodulin-I resulted in enhanced vascular endothelial growth factor (VEGF)-A expression, lipid deposition, and calcification in the cardiac valves of aged mice. In human VHDs, including infective endocarditis, rheumatic heart disease, and atherosclerosis, VEGF-A expression, neovascularization, and calcification were observed in areas of chondromodulin-I downregulation. These findings provide evidence that chondromodulin-I plays a pivotal role in maintaining normal valvular function by preventing angiogenesis that might lead to VHD.

Received March 15, 2008; accepted July 23, 2008.

From the Departments of Regenerative Medicine and Advanced Cardiac Therapeutics (N.K., D.H., M.Y., K.F.), Cardiovascular Surgery (N.K., R.Y.), and Pathology (T.K., Y.O.), Keio University School of Medicine, Tokyo, Japan; Department of Cellular Differentiation, Institute for Frontier Medical Sciences, Kyoto University, Kyoto, Japan (C.S., S.M., Y.H.); Department of Molecular Medicine, Max Planck Institute of Biochemistry, Martinstried, Germany (D.D.); Department of Cardiovascular Surgery, Heart Institute of Japan, Tokyo Women's Medical University, Tokyo, Japan (G.M., T.S.); and Departments of Cardiovascular Surgery (J.K.) and Pathology (H.I.-U.), National Cardiovascular Center Hospital, Osaka, Japan.

The online-only Data Supplement is available with this article at http://circ.ahajournals.org/cgi/content/full/CIRCULATIONAHA.108.780031/DC1.

GenBank accession number: murine tenomodulin, NM_022322.

Correspondence to Keiichi Fukuda, MD, PhD, 35 Shinanomachi, Shinjuku, Tokyo 160-8582, Japan. E-mail kfukuda@sc.itc.keio.ac.jp

Circulation is available at http://circ.ahajournals.org

DOI: 10.1161/CIRCULATIONAHA.108.780031

Editorial p 1694
Clinical Perspective p 1747

Rupture of the CTC is a well-known cause of mitral regurgitation. To elucidate the molecular mechanism, we investigated the expression of chondromodulin-I in the CTC. Unexpectedly, both normal and ruptured CTC lacked expression of chondromodulin-I, suggesting that the mechanism underlying the avascularity or protective function of the CTC differed from that operating in cardiac valves, even though the cardiac valves and CTC lie in proximity to each other and have a similar avascular appearance. The atrioventricular valve leaflets and CTC comprise diverse cell lineages and highly organized matrices that are populated by cartilage[10,11] and tendon[12,13] cell types, respectively. The cartilage cell markers aggrecan and Sox9 are observed in valvular leaflets during embryogenic valvulogenesis, whereas the tendon-associated genes *Scleraxis* and *Tenascin* are expressed in the CTC.[14,15] On the basis of these observations and our previous findings regarding chondromodulin-I in cardiac valves,[9] we speculated that CTC avascularity might be related to the avascular properties of tendon rather than those of cartilage.

Recently, we isolated tenomodulin, which is a novel chondromodulin-I–related gene with 33% amino acid identity. Tenomodulin is a 317–amino acid glycoprotein found in hypovascular tissues, such as tendons, ligaments, the epimysium, and eyes.[16–19] Tenomodulin contains BRICHOS and cysteine-rich domains[20] and has antiangiogenic activities. It is processed in vivo in certain tissues, and the proteolytically cleaved, 16-kDa C-terminal domain promotes tenocyte proliferation.[21,22] In the present study, we investigated whether tenomodulin is expressed in the CTC and its potential involvement in CTC avascularity. We also investigated the cause of the rupture of CTC by comparing the normal and ruptured CTC from the viewpoint of angiogenesis and the involvement of tenomodulin.

Methods

Animals

Wild-type ICR mice were purchased from Japan CLEA (Tokyo, Japan). Japanese White rabbits were purchased from Sankyo Laboratory Service Corporation (Tokyo, Japan). Porcine eyes and hearts were purchased from a public slaughterhouse (Tokyo, Japan). Adult beagle dogs were purchased from NARC Corporation (Chiba, Japan). All experimental procedures and protocols were approved by the animal care and use committees of Keio University and conformed to the National Institutes of Health *Guidelines for the Care and Use of Laboratory Animals*.

Reverse Transcription Polymerase Chain Reaction

Total RNA was isolated with the use of Trizol reagent (GIBCO-BRL) and treated with DNase I (Roche). Reverse transcription polymerase chain reaction (RT-PCR) was performed as described previously[9] with the following primers: murine tenomodulin, 5′-AGAATGAGCAATGGGTGGTC-3′ (forward), 3′-CTCGACCTCCTTGGTAGCAG-5′ (reverse); murine GAPDH, 5′-TTCAACGGCACAGTCAAGG-3′ (forward), 3′-CATGGACTGTGGTCATGAG-5′ (reverse); porcine tenomodulin, 5′-GGTGGTCCCTCAAGTGAAAG-3′ (forward), 3′-CTCGTCCTCCTTGGTAGCAG-5′ (reverse); porcine GAPDH, 5′-TGATGACATCAAGAAGGTGGTGAAG-3′ (forward), 3′-TCCTTGGAGGCCATGTGGACCAT -5′ (reverse).

Immunohistochemical and Immunofluorescence Staining

Conceived or nonconceived adult mouse hearts were perfused from the apex with phosphate-buffered saline, perfusion-fixed with 4% paraformaldehyde in phosphate-buffered saline, and used for immunostaining as described previously.[23] The CTC were dissected immersion-fixed overnight at 4°C in 4% paraformaldehyde, and then embedded in paraffin. Before application of the primary antibodies paraffin was removed from the sections in xylene, and the sections were heated in a microwave oven in 10 mmol/L citrate buffer solution (pH 6.0) (Muto Pure Chemicals Co, Japan) for 3 minutes. After sections were rinsed in phosphate-buffered saline, they were incubated with ImmunoBlock (Dainippon Sumitomo Pharma, Osaka, Japan) 1 hour in room air and incubated overnight at 4°C with 5% normal rabbit serum and rabbit polyclonal antibody to tenomodulin,[17,21] rabbit polyclonal antibody to VEGF-A (1:200 dilution; Santa Cruz Biotechnology, Santa Cruz, Calif), von Willebrand factor (vWF) (1:200 dilution; Laboratory Vision Corporation), elastin (1:50 dilution; Elastin Products Co), collagen type I (1:50 dilution; Rockland), matrix metalloproteinase (MMP)-1 (Daiichi Fine Chemical),[24] MMP-2 (Daiichi Fine Chemical),[24] MMP-3 (Daiichi Fine Chemical),[24] MMP-9 (Daiichi Fine Chemical),[24] MMP-13 (1:100 dilution; Biogenesis),[24] CD11b (1:200 dilution; BD PharMingen), CD14 (1:50 dilution; Santa Cruz Biotechnology), and vimentin (1:20 dilution; Sigma-Aldrich, St Louis, Mo). Immunohistochemical signals were detected by applying 0.05% 3,3′-diaminobenzidine tetrahydrochloride (Sigma-Aldrich) containing 0.01% hydrogen peroxide in 0.05 mol/L Tris-buffered saline (pH 7.6) as a chromogenic substrate. The sections were then counterstained with hematoxylin, dehydrated in a graded ethanol series, and mounted in Permount (Fisher Scientific).

For immunofluorescence studies, the sections were incubated with secondary antibodies conjugated with Alexa 488 or Alexa 546 (Molecular Probes, Carlsbad, Calif). Slides were observed under a confocal laser-scanning microscope (LSM 510 META; Carl Zeiss, Chester, Va). Optical sections were obtained at 1024×1024 pixel resolution and analyzed with the use of LSM software (Carl Zeiss). We substituted nonimmune rabbit serum for primary antibodies as a negative control for each immunostaining experiment.

Quantitative analysis of the stained area was performed by converting images to monochrome with optimum saturation and counting the black pixels with the use of NIH Image software.

Isolation of Adult Rabbit CTC Interstitial Cells

The hearts were dissected from anesthetized 12-week-old Japanese White rabbits. Primary culture of the CTC was examined by modifying the protocol for cardiac valvular interstitial cells[25] and Achilles tendons.[26] Briefly, the CTC was rapidly removed, and the superficial endothelial cells were removed by cotton swab, chopped under a stereomicroscope, and used for the explant culture. Pieces that measured 1×1 mm were cut from the tissue, placed in 12-well collagen-coated dishes (Iwaki), and grown in Dulbecco's modified Eagle's medium (Sigma-Aldrich) with 50% fetal bovine serum for 24 hours at 37°C. An additional 1 mL Dulbecco's modified Eagle's medium with 50% fetal bovine serum was added and left for another 24 hours at 37°C. After the medium and tissue pieces were removed, Dulbecco's modified Eagle's medium with 10% fetal bovine serum was added, and the cells were cultivated at 37°C. Medium was changed every 3 days. Conditioned medium was obtained from confluent CTC interstitial cells 3 days after the medium was changed and used in further analyses.

Cell Culture

Human coronary artery endothelial cells (HCAECs) were purchased from Takara Biotechnology, maintained according to the manufacturer's instructions, and used at passages 3 to 5 in the present study.

Human Samples

Samples comprising 16 CTC were collected from 15 patients undergoing mitral valve replacement or plasty due to its rupture and

1 autopsy patient (8 male and 8 female; mean age, 62.4±12.6 years). Samples were fixed immediately after removal in formaldehyde and then embedded in paraffin. For controls, 20 microscopically and macroscopically normal, noncalcified, smooth, and pliable mitral CTC were collected from 12 autopsied patients (10 male and 2 female; mean age, 62.7±16.5 years). The use of autopsied and surgical specimens of human tissue was approved by the institutional review board of Keio University and the National Cardiovascular Research Center.

Filing the Midlayer of CTC in a Canine Model

After administration of light anesthesia with intravenous injection of pentobarbital (30 mg/kg), adult beagle dogs weighing 14 to 16 kg (mean, 15.2±0.6 kg) were intubated, mechanically ventilated with room air by a Harvard respirator, and anesthetized with 3% sevoflurane and nitrous oxide. The right thoracotomy was performed at the fourth intercostal space, followed by generation of a pericardial cradle, and an extracorporeal bypass was created between the superior and inferior vena cava and the ascending aorta with an inline oxygenator. Both hemodynamics and gas exchange were monitored. The right atrium was opened, and the septal cusp of the tricuspid valve was directly shown. The surface of the several CTC of the septal cusp of tricuspid valve was filed out to remove the elastin layer. Then the heart was closed, extracorporeal bypass was removed, and the chest was closed. After 1 or 3 months, the dogs were anesthetized with pentobarbital and euthanized with KCl. The filed CTC were obtained (n=5, each group), and then the histological and immunohistochemical examinations were performed.

Other methods are described in the online-only Data Supplement.

Statistical Analysis

Values are presented as mean±SEM. Statistical significance was evaluated with the unpaired Student *t* test for comparisons between 2 mean values. Multiple comparisons between >3 groups were performed with an ANOVA test. A value of $P<0.05$ was considered significant.

The authors had fully access to and take full responsibility for the integrity of the data. All authors had read and agree to the manuscript as written.

Results

Expression of Tenomodulin in Normal CTC

Initially, we investigated whether tenomodulin was expressed in normal cardiac valves and CTC. Tenomodulin transcripts were first detected in the murine heart at embryonic day 14.5 and were expressed continuously in adulthood (Figure 1A). It was expressed specifically in the CTC but not in the atrium, ventricle, or cardiac valves (Figure 1B). Western blotting with antibodies specific for the C-terminal portion of tenomodulin identified the 45-kDa glycosylated and 40-kDa nonglycosylated forms of tenomodulin in porcine CTC; these proteins were also detected in the eye (Figure 1C). Interestingly, the CTC, but not the eye, was immunopositive for the 16-kDa C-terminal cleaved domain of tenomodulin, suggesting truncation of the C-terminus to produce the secreted form. Western blot analysis for the N-terminal domain of tenomodulin in the CTC revealed strong 29- and 24-kDa bands, as well as faint 45- and 40-kDa bands, whereas the eye contained mainly the 45- and 40-kDa fragments. Taken together, these results indicate that truncation of the C-terminal domain of tenomodulin occurs in a tissue-specific manner and that the truncated N-terminal domain persists in the CTC.

Immunohistochemistry of the murine heart localized tenomodulin to the CTC (Figure I in the online-only Data Supplement). Hematoxylin-eosin (HE) staining (Figure 2A),

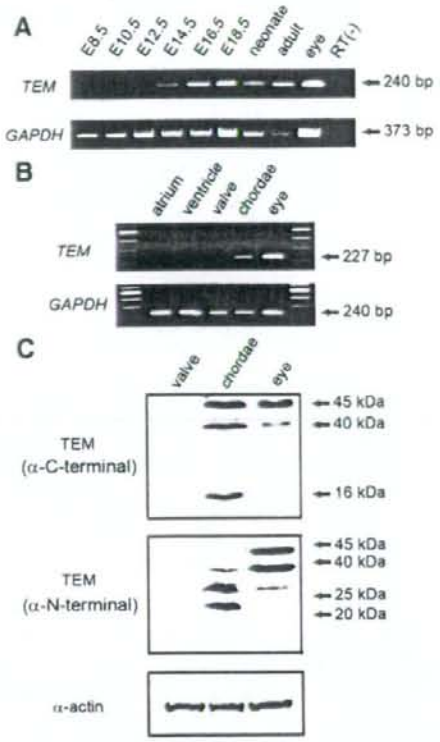

Figure 1. Expression of tenomodulin in CTC. A, Temporal expression of tenomodulin (TEM) in the mouse heart. RT-PCR was performed on samples from embryonic and adult hearts. Positive signals were seen in the embryonic heart from embryonic day (E) 14.5 onward. Adult mouse eyes were used as positive controls. B, RT-PCR of tenomodulin in the porcine heart. Tenomodulin mRNA was specifically expressed in the CTC but not in the atrium, ventricle, or cardiac valves. C, Western blot analysis for tenomodulin in the porcine cardiac valve and CTC with the use of antibody specific for the C-terminus (top panel) and N-terminus (middle panel) of tenomodulin. Eye was used as positive control. Note that the CTC expressed not only 45- and 40-kDa bands but also a 16-kDa band, although the eye expressed only the 45- and 40-kDa bands. This suggests that the C-terminal domain is processed in the CTC but not in the eye.

elastica van Gieson staining (Figure 2B), and immunohistochemistry revealed 3 layers in the normal human CTC, ie, the superficial endothelial layer (Figure 2E), the elastin-rich mid layer (Figure 2G), and the collagen type I–rich core layer (Figure 2H). This structure was consistent with that reported previously.[1] Tenomodulin was restricted to the elastin-rich mid layer (Figure 2C) and was not detected in the other layers. The normal CTC showed no expression of chondromodulin-I (Figure 2D) or VEGF-A (Figure 2F), and there was no abnormal vessel formation. Tenomodulin was deposited at the interstitial space of the elastin-rich layer, although it did not colocalize directly with elastin (Figure 2I).

Tenomodulin Secreted From CTC Interstitial Cells Has Antiangiogenic Activity

We investigated whether CTC interstitial cells produce tenomodulin and the effect that this might have on the tube

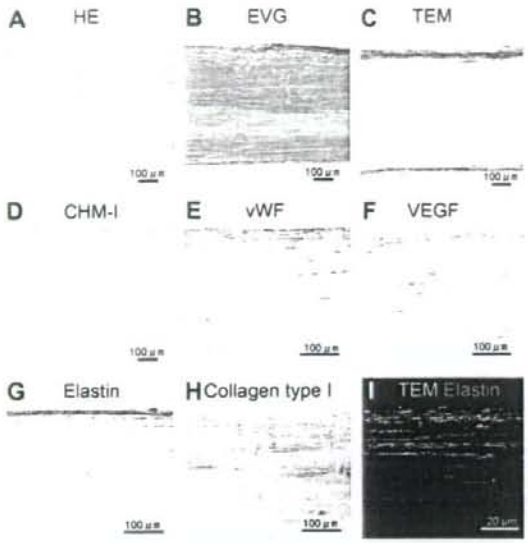

Figure 2. Localization of tenomodulin in normal human CTC. Normal human CTC was investigated by histological and immunohistochemical analyses. A, HE staining. B, Elastica van Gieson (EVG) staining. Immunohistochemistry for normal human CTC with anti-tenomodulin (TEM) (C), anti-chondromodulin-I (CHM-I) (D), anti-vWF (E), anti-VEGF-A (F), anti-elastin (G), and anti-collagen type I (H) antibodies. Tenomodulin was expressed at the elastin-rich mid layer of normal human CTC, and it did not colocalize directly with elastin (I).

morphogenesis of HCAECs. Primary CTC interstitial cells were obtained from explant cultures of rabbit CTC (Figure 3A). The explanted cells formed an orthogonal pattern of overgrowth. These cells were negative for the acetyl-LDL-DiI conjugate, which is consistent with CTC being composed of CTC interstitial cells. Immunostaining detected tenomodulin in the cytoplasm of CTC interstitial cells but not in NIH3T3 cells. RT-PCR confirmed that the cultured CTC interstitial cells expressed tenomodulin and that this expression could be inhibited by treatment with a specific small-interfering RNA (siRNA) (Figure 3B).

The HCAECs showed capillary-like tube formation on Matrigel (Figure 3C). These structures were less apparent after treatment with conditioned medium from CTC interstitial cell cultures (CIC-CM) compared with mock medium or the conditioned medium from NIH3T3 cell cultures (NIH3T3-CM). The HCAECs that were cultured in conditioned medium from siRNA-treated CTC interstitial cells regained the ability to form capillary-like structures. Conditioned media from cultures of NIH3T3 cells transfected with the C-terminal domain of tenomodulin (recombinant protein) similarly inhibited tube formation. Quantitative analysis revealed that CIC-CM inhibited tube formation by 58.3% and that tenomodulin-specific siRNA treatment recovered tube-forming capacity by 38.7% (Figure 3D).

Tenomodulin Secreted From CTC Interstitial Cells Inhibited the Migratory Capacity of the HCAECs

In a modified Boyden chamber, HCAECs cocultured with CTC interstitial cells lost their migratory capacity compared with that cocultured with NIH3T3 cells. Treatment of CTC interstitial cells with tenomodulin-specific siRNA allowed the HCAECs to regain partial migratory capacity (Figure 4A), whereas the control siRNA had no such effect. Coculturing with NIH3T3 cells transfected with the C-terminal domain of tenomodulin similarly inhibited migration. Quantitative analysis showed that CTC interstitial cells decreased the number of migrating cells by 73.2% and that specific siRNA recovered the migratory capacity by 36.6% (Figure 4B). These results imply a pivotal role for tenomodulin as an angiogenesis inhibitor in the CTC.

Marked Downregulation of Tenomodulin and Abnormal Vessel Formation in the Ruptured CTC

We examined specimens from 16 patients with CTC rupture (Figure 5A). The ruptured areas contained numerous large abnormal vessels in the mid layers and core layers, and there was marked tissue degeneration. Elastin was preserved, whereas tenomodulin was markedly downregulated in the ruptured area but not in remote nonruptured areas. These tenomodulin-poor areas expressed VEGF-A and contained the aforementioned large abnormal vessels. In addition, their inner surfaces were coated with vWF-positive endothelial cells rather than smooth muscle cells. Computer image analysis showed that the total cell numbers, vWF-positive cell numbers, and the percentages of VEGF-A–positive areas were markedly increased, whereas the proportions of tenomodulin-positive areas in the ruptured CTC were markedly decreased (Figure 5B to 5E). The adjacent nonruptured CTC obtained at autopsy and during mitral valve replacement revealed normal structures without abnormal vessel formation or aberrant MMP or VEGF-A expression (data not shown). These findings indicated that the CTC ruptures in a fragile area where numerous abnormal vessels are created and tenomodulin expression was locally downregulated.

Expression of MMPs and Cell Infiltration in the Ruptured CTC

The ruptured area of the CTC showed strong expression of MMP-1 and MMP-2 and moderate expression of MMP-13, which corresponded to the expression of VEGF-A (Figure 6A). In contrast, MMP-3 expression was weak, and MMP-9 was not detected. No MMP signals were detected in the normal CTC or in the nonruptured area. High numbers of inflammatory cells positive for CD11b, CD14, and vimentin infiltrated the ruptured area but not the normal CTC or the nonruptured area. The quantitative analyses are shown in Figure 6B to 6E. These findings suggest that abnormal vessel formation in the CTC is accompanied by MMP activation and infiltration of inflammatory cells.

Mechanical Stretching and Hypoxia Suppress the Expression of Tenomodulin by CTC Interstitial Cells

To investigate the cause of tenomodulin downregulation, we investigated whether tenomodulin expression by CTC interstitial cells was affected by various stimuli, such as mechanical stretching, hypoxia, or oxidative stress. CTC interstitial cells would be expected to experience these types of stimuli

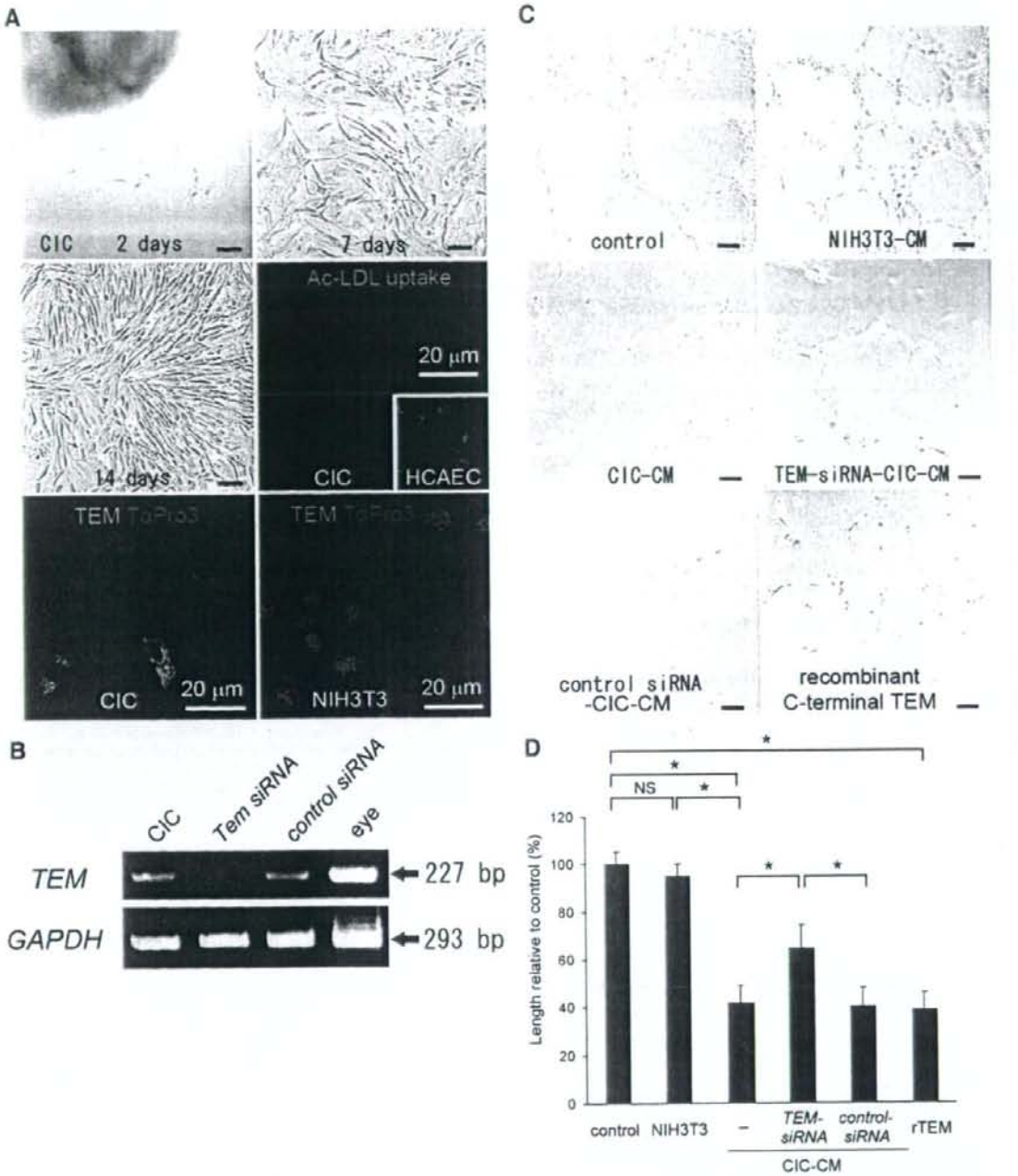

Figure 3. Expression of tenomodulin in CTC interstitial cells and its effect on tube formation in HCAECs. A, Rabbit CTC interstitial cells (CIC) after postexplant culture. At 7 days, CTC interstitial cells showed a cobblestone-like or spindle-like appearance. At 14 days, CTC interstitial cells exhibited a fibroblast-like appearance. Ex indicates explant of CTC. CTC interstitial cells were negative for acetyl-LDL-DiI staining; HCAECs are shown as a positive control (inset). Immunofluorescence staining of tenomodulin (TEM) in rabbit CTC interstitial cells and NIH3T3 cells is shown; nuclei were stained with ToPro-3. B, Effect of siRNA on tenomodulin expression in cultured CTC interstitial cells. RT-PCR for tenomodulin was performed. Lane 1, CIC; lane 2, CIC+siRNA specific to tenomodulin; lane 3, CIC+control siRNA; lane 4, eye for positive control of tenomodulin. C, Tube formation assay. CIC-CM inhibited tube formation of endothelial cells on Matrigel. Representative micrographs of tube formation of HCAECs are shown. Tube formation was significantly suppressed by CIC-CM but not by NIH3T3-CM (negative control). Treatment of CTC interstitial cells with siRNA specific to tenomodulin but not control siRNA reduced the CIC-CM–induced suppression. Recombinant C-terminal tenomodulin represented the conditioned medium of NIH3T3 cells transfected with C-terminal tenomodulin expression plasmids. D, Quantitative analysis of tube lengths in tube formation assay. *$P<0.01$ vs control.

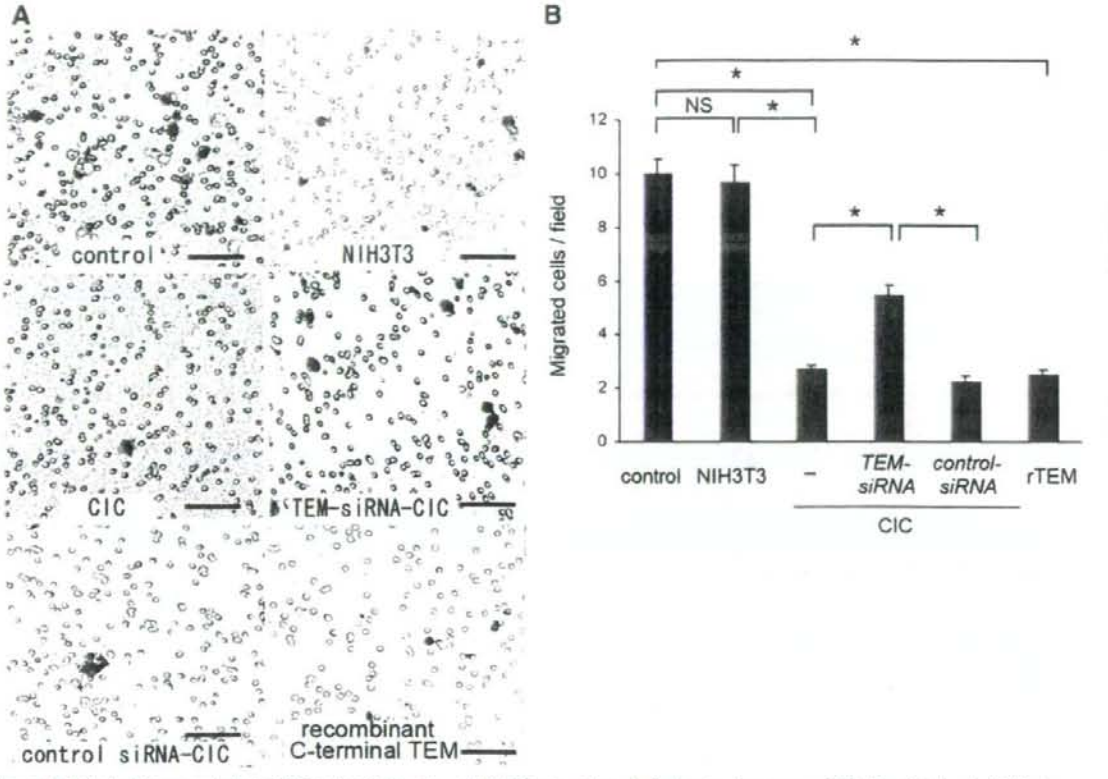

Figure 4. Effect of tenomodulin in CTC interstitial cells on HCAEC migration. A, Cell migration assay. CTC interstitial cells (CIC) abrogated HCAEC chemotaxis in vitro. HCAECs were inhibited from migrating when cocultured with CTC interstitial cells but not when cultured without cells (control) or with NIH3T3 cells (negative control). Treatment of CTC interstitial cells with siRNA specific to tenomodulin (TEM) but not control siRNA reduced the suppression of chemotaxis. Recombinant C-terminal tenomodulin represented the coculture with NIH3T3 cells transfected with C-terminal tenomodulin expression plasmids. B, The graph shows quantitative analysis of the migrated cell numbers in cell migration assay. *$P<0.01$ vs control.

when subjected to abnormal forces (as in hypertension) or during inflammation (as in infective endocarditis). Initially, we stimulated the CTC interstitial cells using a cell-stretching device, and 6 hours later, the expression of tenomodulin was not detectable (Figure IIA in the online-only Data Supplement). Next, CTC interstitial cells were incubated under the hypoxic condition of almost no oxygen. Although the cells were alive, the expression of tenomodulin was not detected as early as 1 hour later (Figure IIB in the online-only Data Supplement). Finally, CTC interstitial cells were treated with several concentrations of antimycin A, which mediates oxidative stress. Tenomodulin expression was observed at an antimycin A concentration <10 μg/mL but was undetectable at 30 μg/mL antimycin A (Figure IIC in the online-only Data Supplement). These findings suggest that various stimuli, such as mechanical stretching, hypoxia, and oxidative stress, cause the down regulation of tenomodulin expression in CTC.

Absence of the Tenomodulin Layer Induces Angiogenesis and MMP Activation

We investigated the effects of the tenomodulin layer on angiogenesis and MMP activation in the collagen-rich core layer. The CTC of the tricuspid valve was examined in an anesthetized canine model, and the tenomodulin-rich layer was removed by filing (Figure 7A). Hemodynamic measurement revealed that there were no significant differences in heart rate, systolic pressure, diastolic pressure, pulmonary arterial pressure, pulmonary capillary wedge pressure, right ventricular systolic pressure, right atrial pressure, and cardiac output between the control (presurgery) dogs and the dogs at 3 months after surgery. Color Doppler echocardiography revealed no significant increases in tricuspid regurgitation at 3 months after surgery.

HE staining and immunostaining for vWF revealed abnormal vessel formation in the core layer next to the surgically filed tenomodulin-deficient area at 3 months (Figure 7B, 7C). Immunohistochemical analyses were performed at 1 and 3 months, at which point the acute inflammation had terminated. VEGF-A, MMP-1, MMP-2, and MMP-13 were observed from 1 month, with their expression extending to ≈15% of the core layer depth (Figure 7D). At 3 months, the expression of these factors was stronger and extended to 37% of the core layer depth. Moreover, abnormal neovascularization was observed only at 3 months, indicating that angiogenesis and MMP activation are caused by loss of the tenomodulin-rich layer rather than operation-induced inflammation (Figure 7E to 7G).

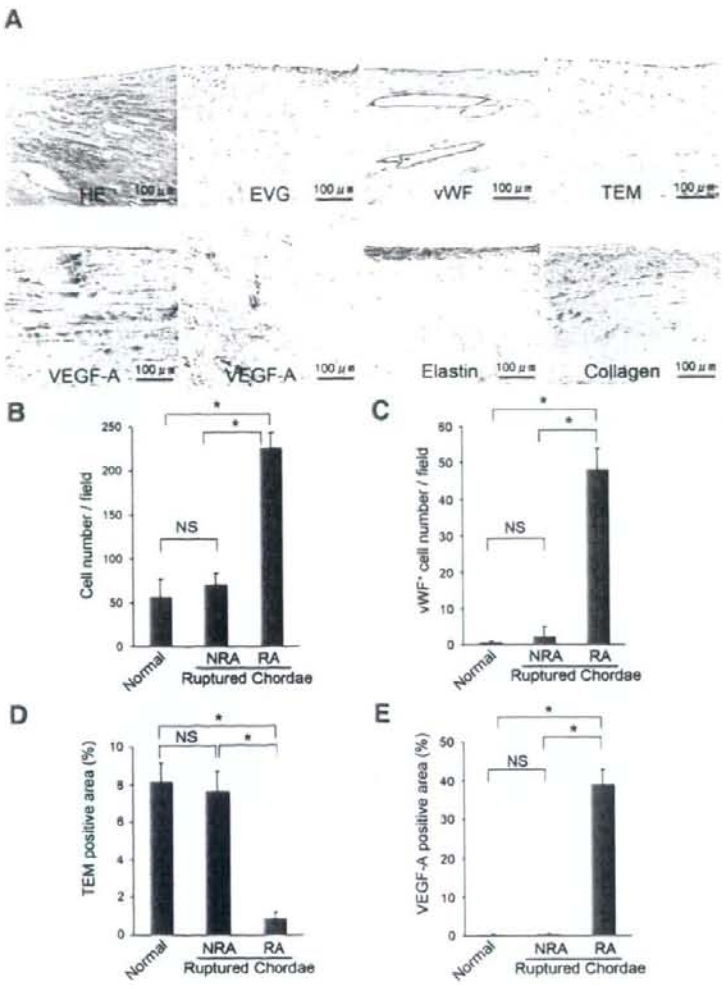

Figure 5. A, Representative histology and immunohistochemistry of the ruptured CTC. Abbreviations are as in Figure 2. The ruptured areas of CTC did not express tenomodulin, whereas they strongly expressed VEGF-A. Note that many abnormal large vessels were apparent in the ruptured area of CTC, and they were covered with vWF+ endothelial cells. Elastica van Gieson (EVG) staining and immunostaining for elastin and collagen type I revealed that the laminar structure was maintained in the ruptured area of CTC, although they were destroyed. B, Quantitative analysis of the number of cells in the normal, nonruptured area (NRA) and ruptured areas (RA) of disrupted CTC. C, Quantitative analysis of the vWF+ cell number. D, Quantitative analysis of the percentage of tenomodulin+ area in normal, NRA, or RA of CTC. E, Quantitative analysis of the percentage of VEGF-A+ area in normal, NRA, or RA of CTC. *$P<0.01$ vs control.

Discussion

Despite their clinical importance, little is known about the mechanisms underlying VHDs.[27-29] The present study reveals a key role for tenomodulin as a potent antiangiogenic factor in the prevention of atrioventricular valvular regurgitation after CTC rupture. We show for the first time that both the C-terminal and N-terminal domains of tenomodulin are expressed persistently in the mid layer of normal CTC, whereas these proteins are downregulated in the diseased CTC. Moreover, the cleaved C-terminal domain of tenomodulin secreted from CTC interstitial cells is a critical antagonist of angiogenesis. Because cardiac valves are flow-regulating tissues in a dynamic chambered pump, the CTC are subjected to mechanical stress[30] and damage to the endothelial cell lining of the outer layer. Tenomodulin probably protects the CTC from the inflammation and vascularization that result from mechanical damage. To confirm this hypothesis, we analyzed the tenomodulin expression profiles of the CTC in the normal and diseased states.

The observed expression patterns and biological activities suggest that tenomodulin protects against both angiogenesis and degeneration of the core layer, analogous to the surface coating applied to steel to prevent internal corrosion. Indeed, observations of the ruptured CTC revealed that VEGF-A and MMPs were strongly activated with increased formation of abnormal vessels, resulting in degeneration of the CTC. More importantly, these areas of degeneration corresponded to regions of local absence of tenomodulin. The dog experiments clearly support our hypothesis that angiogenesis and degeneration occur progressively in areas from which the tenomodulin layer has been removed. These findings suggest that CTC rupture is not accidental but can occur when and where the CTC is weakened by angiogenesis, MMP activation, and the infiltration of inflammatory cells secondary to the loss of or damage to the tenomodulin layer. The molecular mechanism through which a local deficit of tenomodulin causes VEGF-A expression remains unknown. We assume that

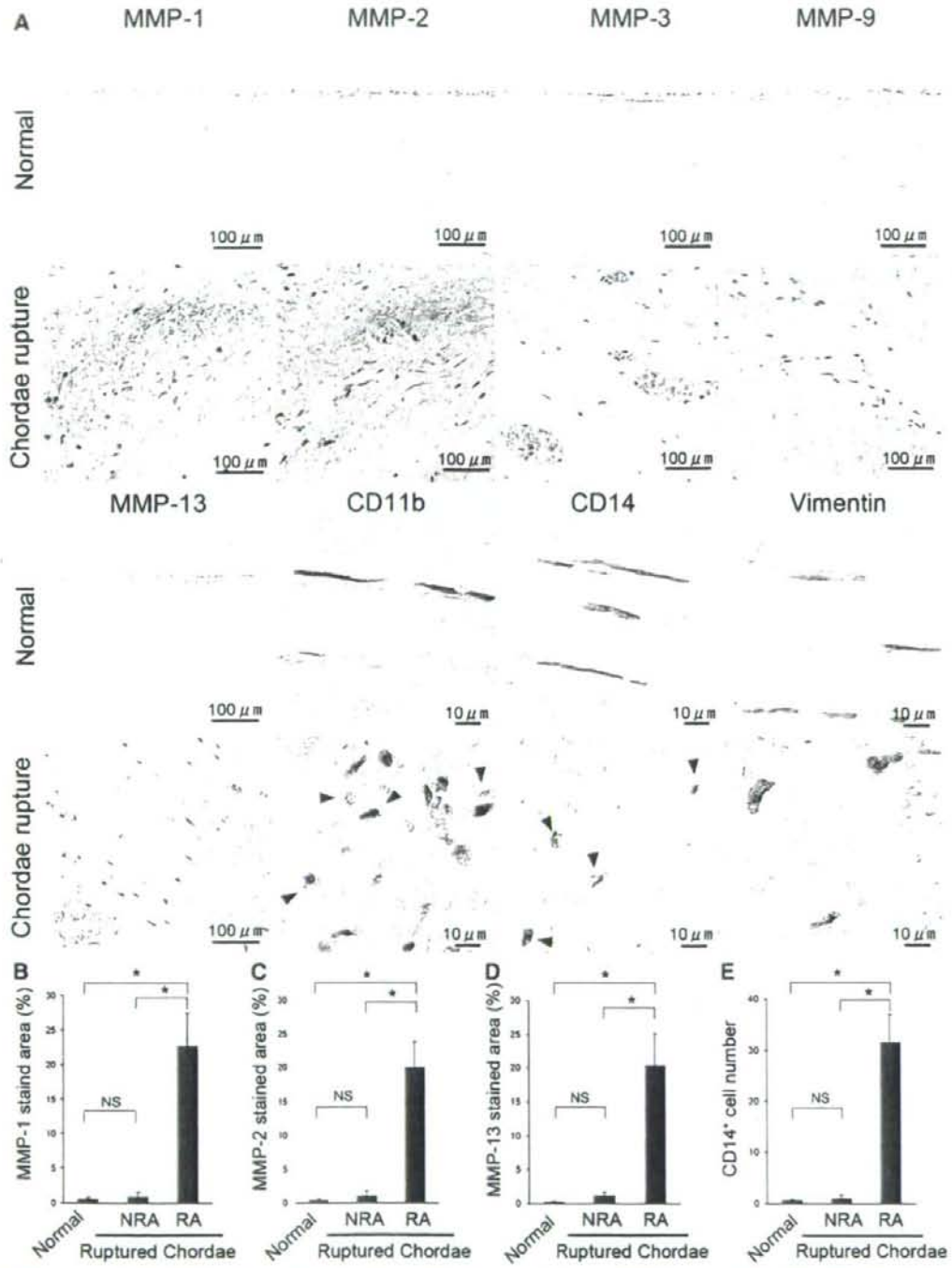

Figure 6. A, Immunohistochemistry of CTC from human autopsies and surgical samples with the use of anti-MMP-1, -MMP-2, -MMP-3, -MMP-9, -MMP-13, -CD11b, -CD14, and -vimentin antibodies. Normal represented the samples from autopsies with normal CTC. The chordae rupture represented the ruptured area of the CTC from surgical samples. B, Quantitative analysis of the percentage of MMP-1–immunostained area in the normal autopsied sample, the nonruptured area (NRA), and ruptured area (RA) of surgical CTC specimen. C, Quantitative analysis of the percentage of MMP-2–immunostained area. D, Quantitative analysis of the percentage of MMP-13–immunostained area. E, Quantitative analysis of the number of $CD14^+$ cells in CTC. *$P<0.01$ vs control.

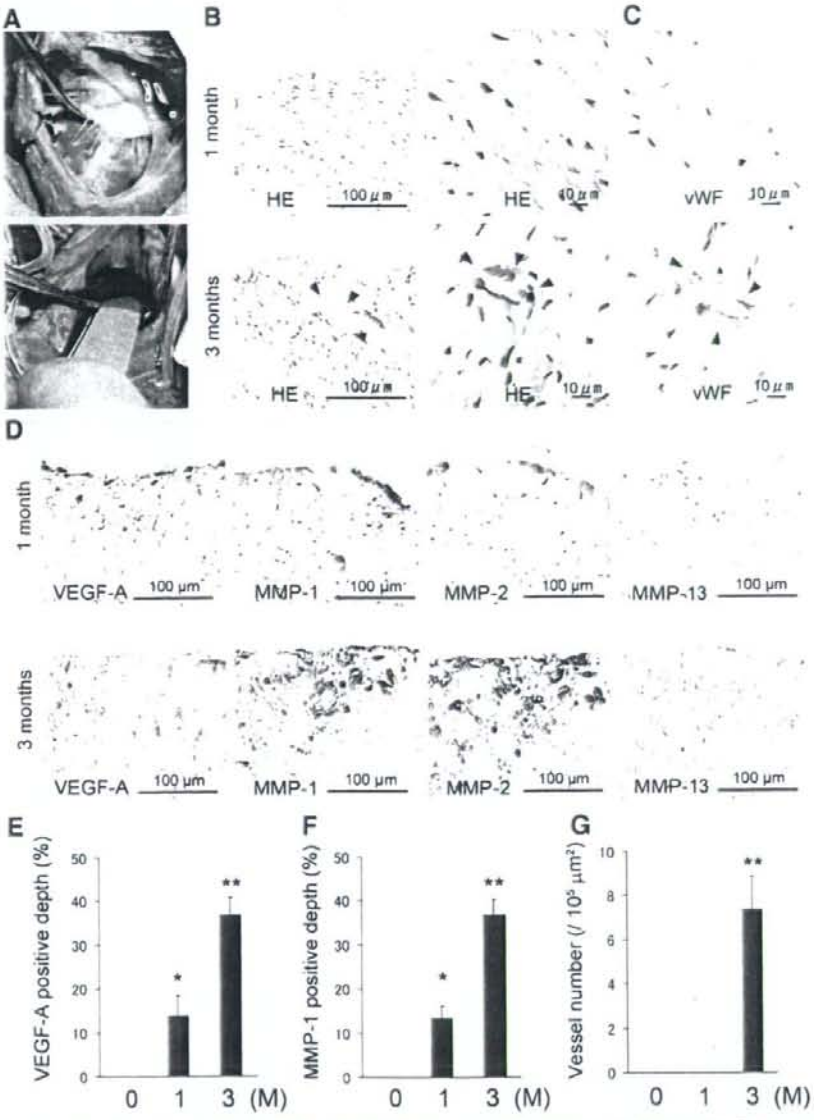

Figure 7. A, Operator's view of the CTC in the tricuspid valve (the septal cusp) in canine model (top panel). The superficial and mid layers of CTC were removed by filing (bottom panel). B, HE staining of the CTC at 1 and 3 months. Note that abnormal small vessel was observed at 3 months. C, Immunohistochemistry for vWF on CTC. Abnormal vessel at 3 months was covered with vWF$^+$ endothelial cells. D, Immunohistochemistry for VEGF-A, MMP-1, MMP-2, and MMP-13 is demonstrated. E, Quantitative analysis for VEGF-A–positive depth compared with the depth of core layer. M indicates month. F, Quantitative analysis for MMP-1–positive depth compared with the depth of core layer. G, Quantitative analysis of the abnormal vessel numbers. $^*P<0.01$, $^{**}P<0.01$ vs control (sham operation, 0 month).

either the downregulation of tenomodulin in CTC interstitial cells or the loss of tenomodulin-producing cells owing to long-standing mechanical stress or inflammation leads to the infiltration of endothelial cells and inflammatory cells, resulting in the activation of MMPs and the expression of VEGF-A. Tenomodulin plays a major role as an antiangiogenic factor in CTC; however, our present data do not exclude the possibility of the existence of other antiangiogenic factors. This should be clarified in the future. We propose that tenomodulin loss occurs after (1) acute inflammation, as in infective endocarditis and rheumatic fever, and (2) excessive mechanical stress to valves, as in trauma, hypertension,[31] and mitral valve prolapse.

The Achilles tendon is one of the most common sites of rupture. It ruptures spontaneously in the majority of patients, without substantial trauma.[32] Local vascularization is implicated in the etiology of this rupture[33,34]; high levels of VEGF-A are expressed by the tenocytes of

ruptured Achilles tendons but not by the tenocytes of normal adult Achilles tendons.[35,36] Hypercellularity, marked vessel formation, and increased MMP expression lead to weakening of the normal tendon structure and subsequent decrease in the mechanical strain tolerance, leading to spontaneous rupture.[36,37] The similarities between these earlier findings and those of the present study suggest that locally augmented mechanical stress or inflammation causes local defects in tenomodulin and induces VEGF-A expression, which may lead to MMP activation, angiogenesis, and degeneration of the CTC to the extent that it ruptures. The present findings support the notion of preclinical investigations of tenomodulin and proteins of similar function as therapeutic agents for the prevention of VHD due to rupture or elongation of the CTC. Understanding these mechanisms should form the basis for new therapeutic regimens for the treatment of VHD.

Sources of Funding

This study was supported in part by research grants from the Ministry of Education, Science, and Culture, Japan, and by the Program for Promotion of Fundamental Studies in Health Science of the National Institute of Biomedical Innovation, Japan.

Disclosures

None.

References

1. Millington-Sanders C, Meir A, Lawrence L, Stolinski C. Structure of chordae tendineae in the left ventricle of the human heart. *J Anat*. 1998;192:573–581.
2. Soini Y, Salo T, Satta J. Angiogenesis is involved in the pathogenesis of nonrheumatic aortic valve stenosis. *Hum Pathol*. 2003;34:756–763.
3. Yamauchi R, Tanaka M, Kume N, Minami M, Kawamoto T, Togi K, Shimaoka T, Takahashi S, Yamaguchi J, Nishina T, Kitaichi M, Komeda M, Manabe T, Yonehara S, Kita T. Upregulation of SR-PSOX/CXCL16 and recruitment of CD8+ T cells in cardiac valves during inflammatory valvular heart disease. *Arterioscler Thromb Vasc Biol*. 2004;24:282–287.
4. Mohler ER III, Gannon F, Reynolds C, Zimmerman R, Keane MG, Kaplan FS. Bone formation and inflammation in cardiac valves. *Circulation*. 2001;103:1522–1528.
5. Hiraki Y, Inoue H, Iyama K, Kamizono A, Ochiai M, Shukunami C, Iijima S, Suzuki F, Kondo J. Identification of chondromodulin I as a novel endothelial cell growth inhibitor: purification and its localization in the avascular zone of epiphyseal cartilage. *J Biol Chem*. 1997;272:32419–32426.
6. Hiraki Y, Kono T, Sato M, Shukunami C, Kondo J. Inhibition of DNA synthesis and tube morphogenesis of cultured vascular endothelial cells by chondromodulin-I. *FEBS Lett*. 1997;415:321–324.
7. Nakamichi Y, Shukunami C, Yamada T, Aihara K, Kawano H, Sato T, Nishizaki Y, Yamamoto Y, Shindo M, Yoshimura K, Nakamura T, Takahashi N, Kawaguchi H, Hiraki Y, Kato S. Chondromodulin I is a bone remodeling factor. *Mol Cell Biol*. 2003;23:636–644.
8. Yamana K, Wada H, Takahashi Y, Sato H, Kasahara Y, Kiyoki M. Molecular cloning and characterization of CHM1L, a novel membrane molecule similar to chondromodulin-I. *Biochem Biophys Res Commun*. 2001;280:1101–1106.
9. Yoshioka M, Yuasa S, Matsumura K, Kimura K, Shiomi T, Kimura N, Shukunami C, Okada Y, Mukai M, Shin H, Yozu R, Sata M, Ogawa S, Hiraki Y, Fukuda K. Chondromodulin-I maintains cardiac valvular function by preventing angiogenesis. *Nat Med*. 2006;12:1151–1159.
10. Chimal-Monroy J, Rodriguez-Leon J, Montero JA, Ganan Y, Macias D, Merino R, Hurle JM. Analysis of the molecular cascade responsible for mesodermal limb chondrogenesis: Sox genes and BMP signaling. *Dev Biol*. 2003;257:292–301.
11. Lincoln J, Alfieri CM, Yutzey KE. Development of heart valve leaflets and supporting apparatus in chicken and mouse embryos. *Dev Dyn*. 2004;230:239–250.
12. Chiquet M, Fambrough DM. Chick myotendinous antigen: a monoclonal antibody as a marker for tendon and muscle morphogenesis. *J Cell Biol*. 1984;98:1926–1936.
13. Schweitzer R, Chyung JH, Murtaugh LC, Brent AE, Rosen V, Olson EN, Lassar A, Tabin CJ. Analysis of the tendon cell fate using Scleraxis, a specific marker for tendons and ligaments. *Development*. 2001;128:3855–3866.
14. Lincoln J, Alfieri CM, Yutzey KE. BMP and FGF regulatory pathways control cell lineage diversification of heart valve precursor cells. *Dev Biol*. 2006;292:292–302.
15. Zhao B, Etter L, Hinton RB Jr, Benson DW. BMP and FGF regulatory pathways in semilunar valve precursor cells. *Dev Dyn*. 2007;236:971–980.
16. Shukunami C, Oshima Y, Hiraki Y. Molecular cloning of tenomodulin, a novel chondromodulin-I related gene. *Biochem Biophys Res Commun*. 2001;280:1323–1327.
17. Oshima Y, Shukunami C, Honda J, Nishida K, Tashiro F, Miyazaki J, Hiraki Y, Tano Y. Expression and localization of tenomodulin, a transmembrane type chondromodulin-I-related angiogenesis inhibitor, in mouse eyes. *Invest Ophthalmol Vis Sci*. 2003;44:1814–1823.
18. Shukunami C, Oshima Y, Hiraki Y. Chondromodulin-I and tenomodulin: a new class of tissue-specific angiogenesis inhibitors found in hypovascular connective tissues. *Biochem Biophys Res Commun*. 2005;333:299–307.
19. Shukunami C, Takimoto A, Oro M, Hiraki Y. Scleraxis positively regulates the expression of tenomodulin, a differentiation marker of tenocytes. *Dev Biol*. 2006;298:234–247.
20. Hiraki Y, Shukunami C. Angiogenesis inhibitors localized in hypovascular mesenchymal tissues: chondromodulin-I and tenomodulin. *Connect Tissue Res*. 2005;46:3–11.
21. Docheva D, Hunziker EB, Fassler R, Brandau O. Tenomodulin is necessary for tenocyte proliferation and tendon maturation. *Mol Cell Biol*. 2005;25:699–705.
22. Oshima Y, Sato K, Tashiro F, Miyazaki J, Nishida K, Hiraki Y, Tano Y, Shukunami C. Anti-angiogenic action of the C-terminal domain of tenomodulin that shares homology with chondromodulin-I. *J Cell Sci*. 2004;117:2731–2744.
23. Funaki H, Sawaguchi S, Yaoeda K, Koyama Y, Yaoita E, Funaki S, Shirakashi M, Oshima Y, Shukunami C, Hiraki Y, Abe H, Yamamoto T. Expression and localization of angiogenic inhibitory factor, chondromodulin-I, in adult rat eye. *Invest Ophthalmol Vis Sci*. 2001;42:1193–1200.
24. Fujimoto N, Iwata K. Use of EIA to measure MMPs and TIMPs. *Methods Mol Biol*. 2001;151:347–358.
25. Zacks S, Rosenthal A, Granton B, Havenith M, Opas M, Gotlieb AI. Characterization of Cobblestone mitral valve interstitial cells. *Arch Pathol Lab Med*. 1991;115:774–779.
26. Pufe T, Petersen W, Kurz B, Tsokos M, Tillmann B, Mentlein R. Mechanical factors influence the expression of endostatin—an inhibitor of angiogenesis—in tendons. *J Orthop Res*. 2003;21:610–616.
27. Chalajour F, Treede H, Ebrahimnejad A, Lauke H, Reichenspurner H, Ergun S. Angiogenic activation of valvular endothelial cells in aortic valve stenosis. *Exp Cell Res*. 2004;298:455–464.
28. Freed LA, Acierno JS Jr, Dai D, Leyne M, Marshall JE, Nesta F, Levine RA, Slaugenhaupt SA. A locus for autosomal dominant mitral valve prolapse on chromosome 11p15.4. *Am J Hum Genet*. 2003;72:1551–1559.
29. Sedransk KL, Grande-Allen KJ, Vesely I. Failure mechanics of mitral valve chordae tendineae. *J Heart Valve Dis*. 2002;11:644–650.
30. Rodriguez F, Langer F, Harrington KB, Tibayan FA, Zasio MK, Cheng A, Liang D, Daughters GT, Covell JW, Criscione JC, Ingels NB, Miller DC. Importance of mitral valve second-order chordae for left ventricular geometry, wall thickening mechanics, and global systolic function. *Circulation*. 2004;110:II115–II122.
31. Lin TH, Su HM, Voon WC, Lai HM, Yen HW, Lai WT, Sheu SH. Association between hypertension and primary mitral chordae tendinae rupture. *Am J Hypertens*. 2006;19:75–79.
32. Jozsa LG, Kannus P. *Human Tendons: Anatomy, Physiology, and Pathology*. Champaign, Ill: Human Kinetics; 1997.
33. Movin T, Gad A, Reinholt FP, Rolf C. Tendon pathology in long-standing achillodynia: biopsy findings in 40 patients. *Acta Orthop Scand*. 1997;68:170–175.

34. Kannus P, Jozsa L. Histopathological changes preceding spontaneous rupture of a tendon: controlled study of 891 patients. *J Bone Joint Surg Am.* 1991;73:1507–1525.
35. Pufe T, Petersen W, Tillmann B, Mentlein R. The angiogenic peptide vascular endothelial growth factor is expressed in foetal and ruptured tendons. *Virchows Arch.* 2001;439:579–585.
36. Pufe T, Petersen WJ, Mentlein R, Tillmann BN. The role of vasculature and angiogenesis for the pathogenesis of degenerative tendons disease. *Scand J Med Sci Sports.* 2005;15:211–222.
37. Tallon C, Maffulli N, Ewen SW. Ruptured Achilles tendons are significantly more degenerated than tendinopathic tendons. *Med Sci Sports Exerc.* 2001;33:1983–1990.

CLINICAL PERSPECTIVE

Valvular heart disease is a life-threatening disease. Although the overall incidence of rheumatic valvular heart disease has been decreasing continuously in developed countries, it has increased with respect to patient age. Rupture of the chordae tendineae cordis (CTC) is a well-known cause of mitral regurgitation, although its etiology remains unknown and surgical procedures have focused exclusively on treatment. Cardiac valves and the CTC are avascular tissues, and we have recently reported that cardiac valves express chondromodulin-I, which is an angioinhibitory factor purified from cartilage that plays a pivotal role in the maintenance of normal valvular function by preventing angiogenesis. In the present study, we show that tenomodulin, which is a chondromodulin-I–related antiangiogenic factor isolated from tendons, is concentrically expressed in normal CTC. Conditioned medium from cultured CTC interstitial cells showed a strong angioinhibitory effect, and the immunohistochemical analysis of human surgical samples showed that tenomodulin was locally absent in the ruptured areas of the CTC, in which abnormal vessel formation, strong expression of vascular endothelial growth factor-A and matrix metalloproteinases, and infiltration of inflammatory cells were observed, whereas these features were not observed in the normal or nonruptured areas. The tenomodulin layers of the tricuspid CTC of dogs were surgically filed, the animals were euthanized after several months, and immunohistological analyses were performed. Angiogenesis and the expression of vascular endothelial growth factor-A and matrix metalloproteinases in the core layer were observed in a time-dependent manner. The present findings support tenomodulin and unknown proteins of similar function as therapeutic agents for the prevention of CTC rupture. Understanding these mechanisms should form the basis for new therapeutic regimens for the treatment of valvular heart disease.

Biochemical and Biophysical Research Communications 369 (2008) 801–806

Contents lists available at ScienceDirect

Biochemical and Biophysical Research Communications

journal homepage: www.elsevier.com/locate/ybbrc

Common marmoset embryonic stem cell can differentiate into cardiomyocytes

Hao Chen [a,b], Fumiyuki Hattori [a,c], Mitsushige Murata [a,b], Weizhen Li [a], Shinsuke Yuasa [a], Takeshi Onizuka [a,b], Kenichiro Shimoji [a,b], Yohei Ohno [a,b], Erika Sasaki [d], Kensuke Kimura [a,b], Daihiko Hakuno [a,b], Motoaki Sano [a], Shinji Makino [a], Satoshi Ogawa [b], Keiichi Fukuda [a,*]

[a] Department of Regenerative Medicine and Advanced Cardiac Therapeutics, Keio University School of Medicine, 35 Shinanomachi, Shinjuku-ku, Tokyo 160-8582, Japan
[b] Division of Cardiology, Department of Medicine, Keio University School of Medicine, 35 Shinanomachi, Shinjuku-ku, Tokyo 160-8582, Japan
[c] Asubio Pharma Co., Ltd., 1-1-1 Wakayamadai, Shimamoto-cho, Mishima-gun, Osaka 618–8513, Japan
[d] Laboratory of Applied Developmental Biology, Marmoset Research Department, Central Institute for Experimental Animals, 1430 Nogawa, Miyamae-ku, Kawasaki, Kanagawa 216-0001, Japan

ARTICLE INFO

Article history:
Received 7 February 2008
Available online 10 March 2008

Keywords:
Embryonic stem cell
Common marmoset
Primate
Monkey
Cardiomyocytes
Differentiation
Characterization
Heart regeneration
Preclinical model

ABSTRACT

Common marmoset monkeys have recently attracted much attention as a primate research model, and are preferred to rhesus and cynomolgus monkeys due to their small bodies, easy handling and efficient breeding. We recently reported the establishment of common marmoset embryonic stem cell (CMESC) lines that could differentiate into three germ layers. Here, we report that our CMESC can also differentiate into cardiomyocytes and investigated their characteristics. After induction, *FOG-2* was expressed, followed by *GATA4* and *Tbx20*, then *Nkx2.5* and *Tbx5*. Spontaneous beating could be detected at days 12–15. Immunofluorescent staining and ultrastructural analyses revealed that they possessed characteristics typical of functional cardiomyocytes. They showed sinus node-like action potentials, and the beating rate was augmented by isoproterenol stimulation. The BrdU incorporation assay revealed that CMESC-derived cardiomyocytes retained a high proliferative potential for up to 24 weeks. We believe that CMESC-derived cardiomyocytes will advance preclinical studies in cardiovascular regenerative medicine.

Cardiomyocytes have been known to terminally differentiate and lose their ability to proliferate soon after birth [1]. Some researchers have reported the possible existence of adult cardiac stem or progenitor cells [2–4], but unfortunately these cells do not have sufficient proliferation ability for repairing the damaged heart [5]. Therefore, once the physical or functional loss of myocytes occurs due to myocardial infarction (MI) or myocarditis, a damaged heart cannot recover its structure and function. The characteristics of embryonic stem (ES) cells include clonal and unlimited expansion, as well as differentiation into various cell types including cardiomyocytes [6]. Thus, human ES cells would be an attractive cell source for regenerative heart therapy. However, before these can be applied clinically, the therapeutic efficacy and safety of ES cell-derived cardiomyocytes must be proven in preclinical experiments using a primate model system.

To date, rhesus and cynomolgus monkeys have been the most frequently used primate models in preclinical studies. Recently, the common marmoset monkey (*Callithrix jacchus*) has attracted a great deal of attention as a potential laboratory and preclinical experimental animal, because it has many advantages including a small body, a short gestation period (approximately 144 days), early sexual maturity (12–18 months), bears 4–6 progeny/year, is cost efficient and is easy to maintain. Recently, we reported the establishment of three CMESC lines, which have many similarities to human ES cells including morphology, surface antigens and cellular characteristics [7]. It is expected that common marmoset monkeys and CMESC-derived differentiated cells will provide a powerful preclinical model for studies in the field of regenerative medicine.

Rhesus and cynomolgus monkey ES cells have already been established [8,9], and these ES cells are able to differentiate into cardiomyocytes [10,11]. We have reported previously that CMESC lines can differentiate into neuron and glia, and induce formation of teratomas including cartilage, adipose tissue, skeletal muscle, a bronchus-like structure, keratinizing squamous epidermis, epidermis and CD31-positive vascular endothelial cells [7]. However, we were not able to induce cardiomyocyte differentiation from CMESC.

To utilize this system for preclinical studies into heart regeneration, we investigated conditions that were suitable for cardiomyocyte induction from CMESC. Here we report the successful

* Corresponding author. Address: Department of Regenerative Medicine and Advanced Cardiac Therapeutics, Keio University School of Medicine, 35 Shinanomachi, Shinjuku-ku, Tokyo 160-8582, Japan. Fax: +81 3 5363 3875.
E-mail address: kfukuda@sc.itc.keio.ac.jp (K. Fukuda).

0006-291X/$ - see front matter © 2008 Elsevier Inc. All rights reserved.
doi:10.1016/j.bbrc.2008.02.141

differentiation of CMESC into cardiomyocytes. The CMESC-derived cardiomyocytes were characterized in detail.

Materials and methods

Common marmoset ES cell culture and differentiation. The CMESC lines No. 20 and 40 were obtained from the Laboratory of Applied Developmental Biology, Marmoset Research Department, Central Institute for Experimental Animals [7]. CMESCs were cultured on 10 μg/mL mitomycin C-treated mouse embryonic fibroblast (MEF) feeder cells with CMESM (common marmoset ES cell medium) culture medium, which consisted of 80% Knockout Dulbecco's modified Eagle's medium (KO-DMEM; Invitrogen Co., 10829-018) supplemented with 20% Knockout Serum Replacement® (KSR; Invitrogen Co., 10828-028), 0.1 mM MEM Non-Essential Amino Acids Solution (Sigma–Aldrich Co., M7145), 2 mM L-Glutamine (Invitrogen Co., 25030-081), 0.1 mM β-Mercaptoethanol (2-ME; Sigma–Aldrich Co., M-7522) and 4 ng/mL basic fibroblast growth factor (bFGF; Wako Pure Chemical Industries Ltd., 064-04541). CMESCs were passaged every 5 or 6 days to maintain them in an undifferentiated state.

For differentiation, CMESC colonies of an appropriate size were chosen using a combination of 40-μm and 100-μm cell-strainers (Becton–Dickinson) that also facilitated the complete removal of feeder cells. Embryoid bodies (EBs) were formed by suspending and culturing colonies in Petri dishes during the first 10 days. To evaluate the incidence of beating EBs, EBs were distributed in non-adhesive 96-well culture plates (Sumitomo Bakelite Co., Ltd.) with approximately 1–2 EBs per well.

Reverse transcription-polymerase chain reaction (RT-PCR) analysis. Total RNA was prepared from EBs using ISOGEN (Nippon gene Co., Ltd., 317-02501), according to the manufacturer's instructions. Contaminating genomic DNA was degraded by RNase-Free DNase I (Ambion, Japan, #2222) at 37 °C for 30 min. Following phenol–chloroform extraction and ethanol precipitation, total RNA was reverse transcribed into cDNA using the Oligo-(dT)12-18 primer (Superscript II RT kit; Invitrogen Co., 18064-022) and then amplified by PCR using RED-Taq DNA polymerase (Sigma–Aldrich Co., D4309). The primer sequences and PCR conditions are listed online in Supplementary Table 1.

Immunofluorescent staining. EBs (6–8 weeks after differentiation) were fixed in 4% paraformaldehyde for 30 min at room temperature, cryoprotected with sucrose and cryosectioned into 7-μm sections. After pretreatment with ImmunoBlock® (Dainippon Sumitomo Pharma Co., Ltd., KN001), the sections were incubated at 4 °C overnight with the primary antibodies diluted in TBST (Tris-buffered saline with 0.1% Tween 20). The fluorescent dye-conjugated secondary antibodies were then applied to the sections for 30 min at 37 °C. The antibodies used in this study are listed online in Supplementary Table 2. The nuclei were stained with DAPI or ToPro-3 (Invitrogen Co.) and observed by conventional fluorescent microscopy (IX71; Olympus Co.) and confocal Laser microscopy (LSM510 META; Carl Zeiss Inc.), respectively.

Transmission electron microscopy (TEM). EBs were fixed in cold 2.5% glutaraldehyde with 2% paraformaldehyde in 0.1 mol/L cacodylate buffer (pH 7.4), post-fixed in 1% osmium tetroxide, dehydrated and embedded in Epon resin. Ultrathin sections were mounted on copper grids, stained with uranyl acetate and lead citrate, and examined by TEM (Philips).

Electrophysiology. The microscope was equipped with a recording chamber and a noise-free heating plate (Microwarm Plate; Kitazato Supply). A 10 mmol/L volume of HEPES was added to the culture medium to maintain the pH of the perfusate at 7.5–7.6. Standard glass microelectrodes that had a DC resistance of 25–35 MΩ when filled with pipette solution (2 mol/L KCl) were used. The electrodes were positioned using a motor-driven micromanipulator (EMM-3SV; Narishige) under optical control. Spontaneously beating cells were selected as targets, and the action potentials of the targeted cells were recorded. The recording pipette was connected to a patch-clamp amplifier (Axopatch 200B; Axon Instruments), and the signal was passed through a low-pass filter with a cut-off frequency of 2 kHz and digitized with an A/D converter with a sampling frequency of 10 kHz (Digidata 1440A; Axon Instruments). Signals were monitored, recorded as electronic files, and analyzed offline with pCLAMP 10 software (Axon Instruments).

BrdU incorporation assay. After three weeks of differentiation, the medium was changed and EBs were cultured in α-MEM supplemented with 10% FCS. Five to 36-week-old EBs were divided into two groups. EBs in Group 1 (intact EB) were cultured with 10 μmol/L of BrdU for 24 h in α-MEM supplemented with 10% FCS, then fixed with 4% paraformaldehyde. After treatment with 20% sucrose for 1 hour at RT, the fixed cells were cryosectioned. The sections were immersed in 2 N HCl with 0.5% Tween 20 solution for 20 min. Cardiomyocytes that had incorporated BrdU were detected using the BrdU Labeling and Detection Kit I (Roche Diagnostics Co., 11296736001) according to the manufacturer's instructions, except that the primary antibody for Nkx2.5 and the secondary antibody conjugated with Alexa-546 (Invitrogen Co.) were also used to identify cardiomyocytes. EBs in Group 2 (dispersed condition) were dispersed by 0.1% trypsin and 0.1% collagenase type III (Worthington Biochemical Co., #4182) in ADS buffer (116 mM NaCl, 20 mM HEPES, 12.5 mM NaH_2PO_4, 5.6 mM glucose, 5.4 mM KCl, and 0.8 mM $MgSO_4$, pH 7.35) with stirring. After 2 days of culture in α-MEM supplemented with 10% FCS, 10 μmol/L of BrdU was added and the dispersed EBs were cultured for a further 24 h at 37 °C in the same medium. Detection of BrdU-incorporated cardiomyocytes was performed as described above.

Results

Differentiation of CMESCs into spontaneously contracting cardiomyocytes

The two lines of CMESCs were cultured in medium containing KSR instead of animal-derived serum in order to maintain pluripotency (Fig. 1A, left). To stimulate the CMESCs to differentiate into cardiomyocytes, we adopted a conventional floating culture system and tested several combinations of medium (DMEM, KO-DMEM or α-MEM) and several lots of fetal calf serum (FCS) or KSR. We succeeded in stimulating CMESC line No. 20 to differentiate into contracting EBs, but failed to differentiate CMESC line No.40 under all conditions tested. CMESC line No. 20 could differentiate into EBs with contracting areas when a combination of three out of five lots of FCS (5–20% in use) and KO-DMEM or α-MEM were used. Strikingly, beating EBs could be obtained very efficiently by culturing the cells in KO-DMEM supplemented with 20% KSR, which was named dCMESM (common marmoset ES cell medium for cardiomyocyte differentiation). This had the same composition as the CMESM, but lacked bFGF. Confluent cultures of undifferentiated CMESCs were completely dissociated from the feeder cells and cultured in suspension to form EBs in dCMESM. In the floating culture system, CMESCs efficiently developed EBs and spontaneously beating cells (Supplementary Movie). An average of 10–20% of EBs began spontaneously contracting 12–15 days after differentiation. A maximum percentage (46 ± 13%) of contractile EBs was observed at approximately 18 days after differentiation, and was roughly sustained for two months.

Most contractile areas within EBs were located in the cell mass or the periphery of cystic structures. Contraction of CMESC-derived EBs was highly sensitive to temperature, a characteristic shared by human ES-derived EBs. EBs were cryosectioned 6–8 weeks after differentiation and immunofluorescent staining was performed. Typically Nkx2.5 and α-Actinin double-positive areas existed in the subsurface of EBs (Fig. 1A, center and right). In the cardiomyocyte-containing EBs, the Nkx2.5 and α-Actinin double-positive cells were approximately 30% of total cells.

Immunofluorescent staining and microstructure of CMESC-derived cardiomyocytes

Immunofluorescent staining was essential to determine the cardiomyocyte structure and the expression of cardiomyocyte-specific proteins. However, at the start of this study, the type of antibodies that would recognize common marmoset monkey cardiomyocytes was unknown. We therefore tested various antibodies that could detect cardiomyocyte-specific proteins in the CMESC-derived cardiomyocytes. Spontaneously beating EBs were dispersed and the CMESC-derived cardiomyocytes were cultured under adherent culture conditions. Immunofluorescent staining was then performed. Antibodies for the cardiac-specific transcription factors Nkx2.5 and GATA4 strongly labeled the nuclei of the CMESC-derived cardiomyocytes. Moreover, antibodies for α-Actinin, myosin heavy chain (MHC), myosin light chain (MLC) and Tropomyosin strongly labeled the typical myofilament structure of the cardiomyocytes. The antibody for the atrial natriuretic peptide (ANP) highlighted the secretary granules typical of cardiomyocytes surrounding the nucleus (Fig. 1B).

Microstructural analysis using TEM revealed typical myofilament structures, desmosomes and a number of mitochondria in CMESC-derived cardiomyocytes (Fig. 1C).

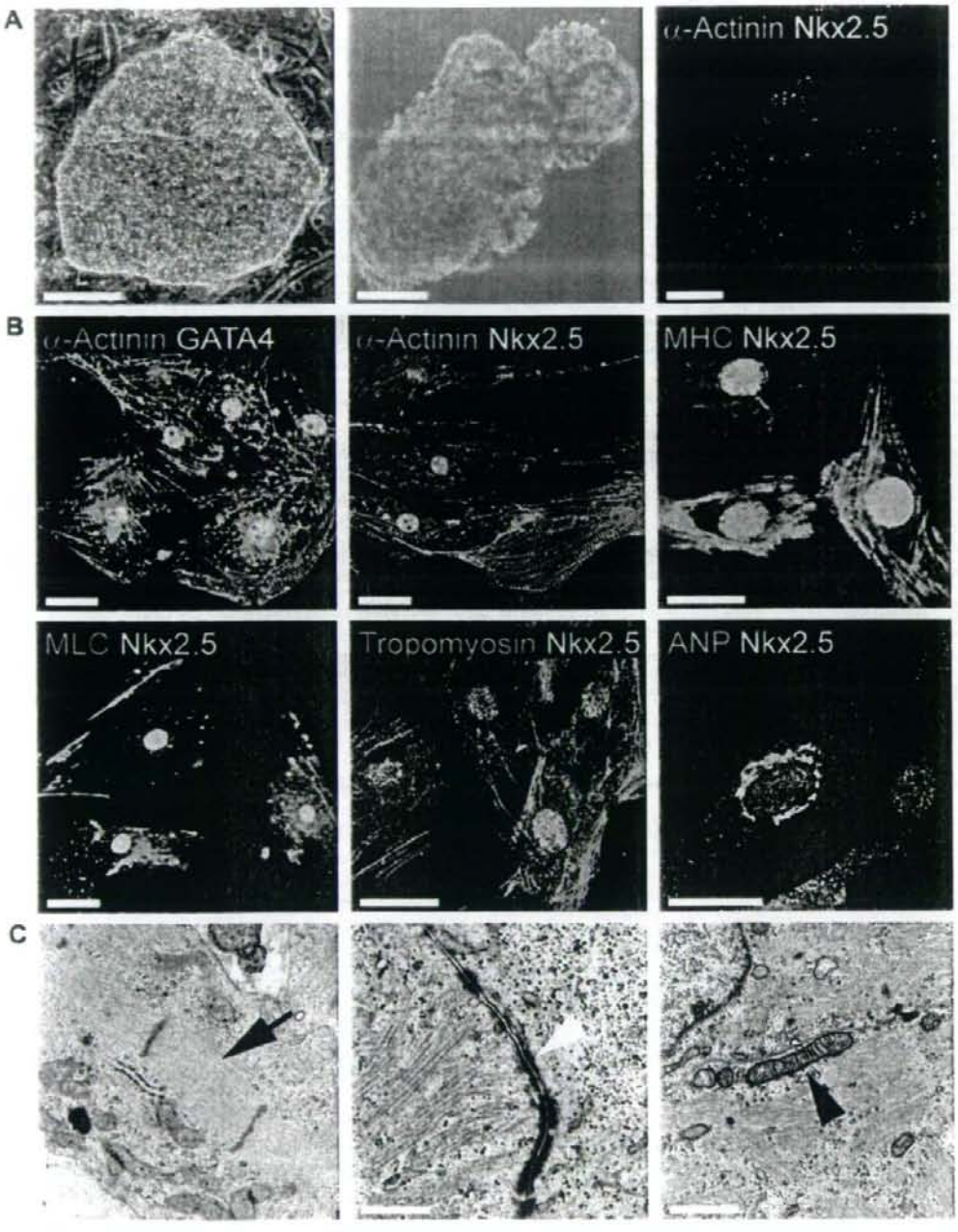

Fig. 1. Structural studies of CMESC-derived cardiomyocytes. (A) Phase contrast microscopy of the undifferentiated CMESC (left), and typical cardiomyocyte-containing non-cystic embryoid body (EB) (center). Immunofluorescent microscopy of cryosections of EBs using anti-α-Actinin and Nkx2.5 antibodies. (B) Double immunofluorescent staining for Nkx2.5 or GATA4 combined with α-Actinin, MHC, MLC, Tropomyosin or ANP. (C) Transmission electron microscopy of the CMESC-derived cardiomyocytes: striated muscle fiber (left, black arrow), desmosomal structure (middle, white arrow head) and mitochondria (right, black arrow head). Scale bars: (A) 100 μm; (B), 20 μm; (C) 0.5 μm.

Time course of marker gene expression during cardiomyocyte differentiation

To characterize the differentiation pathway of undifferentiated CMESC into cardiomyocytes, we performed semi-quantitative RT-PCR to analyze the expression of various marker genes associated with pluripotency, visceral endoderm, and early and late cardiomyogenesis. Some of the primers used have been described previously [7,10], and some were designed based on similar murine, *macaca fascicularis* and *homo sapiens* sequences (Supplementary Table 1). The pluripotency markers *Nanog* and octamer-binding transcription factor 3 (*Oct3/4*) were expressed at high levels in

undifferentiated ES cells. Expression levels of both markers gradually decreased upon differentiation and completely disappeared at day 15 post-differentiation (Fig. 2A). The early mesendoderm marker *Brachyury* was observed from day 3 post-differentiation, peaked at day 6 post-differentiation, but could not be detected at day 9 post-differentiation (Fig. 2B). The visceral endoderm marker alpha-fetoprotein (*AFP*) was observed from day 3 post-differentiation and peaked at day 9 post-differentiation, but could not be detected at day 15 post-differentiation (Fig. 2C). For the genes encoding cardiac-related transcription factors, the expression of the friend of GATA 2 (*FOG-2*) was first observed from day 3 post-differentiation, *GATA4* and the t-box 20 (*Tbx-20*) were from day 6 post-differentiation, *Tbx5* was from day 9 post-differentiation, and *Nkx2.5* was strongly observed at day 15 post-differentiation (Fig. 2D). For the cardiomyocyte-specific proteins, *ANP* and the MLC 2 atrial (*MLC2a*) were observed first from day 6 post-differentiation, *α-MHC* and *β-MHC* were from day 9 post-differentiation, the MLC 2 ventricular (*MLC2v*) was from day 12 post-differentiation (Fig. 2E).

Action potential recordings of CMESC-derived cardiomyocytes

We recorded the action potentials of CMESC-derived cardiomyocytes using glass microelectrodes. Eight-week-old contracting EBs were selected manually and dispersed into small clumps and single cells. The dispersed EBs were cultured to confluence for three days before analysis. The microelectrode was advanced to the intracellular cytoplasm and the voltage of the bulk solution and cytoplasm were measured. Rhythmic beating could be detected in the CMESC-derived cardiomyocytes. The action potential resembled a sinus node, indicating that the CMESC-derived cardiomyocytes had a relatively shallow resting membrane potential, slow diastolic depolarization and relatively long action potential duration (Fig. 3A). The administration of isoproterenol increased their beating rates (Fig. 3B). The basic cycle length (BCL), action potential duration (APD), d*V*/d*t*, action potential amplitude (APA) and maximum diastolic potential (MDP) were also recorded (Fig. 3C).

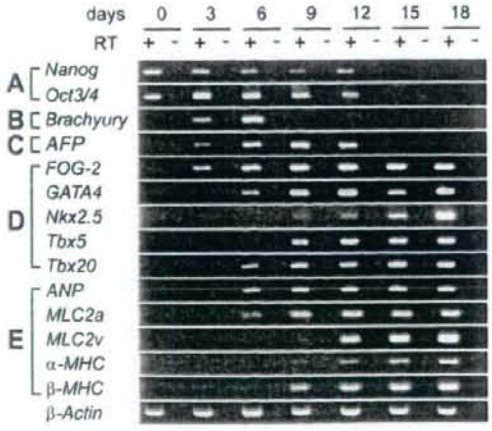

Fig. 2. RT-PCR analysis of the CMESC-derived EBs for various immature and cardiomyocyte-specific proteins. (A) Pluripotency-related genes: *Nanog* and *Oct3/4*; (B) Mesodermal marker gene: *Brachyury*; (C) Primitive endodermal marker gene: *AFP*; (D) cardiomyocyte-precursor and cardiomyocyte marker genes: *FOG-2*, *GATA4*, *Nkx2.5*, *Tbx5*, and *Tbx20*; (E) Cardiomyocyte-associated structural protein genes: *ANP*, *MLC2a*, *MLC2v*, *α-MHC*, *β-MHC*, and equal loading control β-actin. Reverse-transcription negative controls were also amplified and loaded in the lane next to the relevant sample. Abbreviations are listed in Supplementary Table 1.

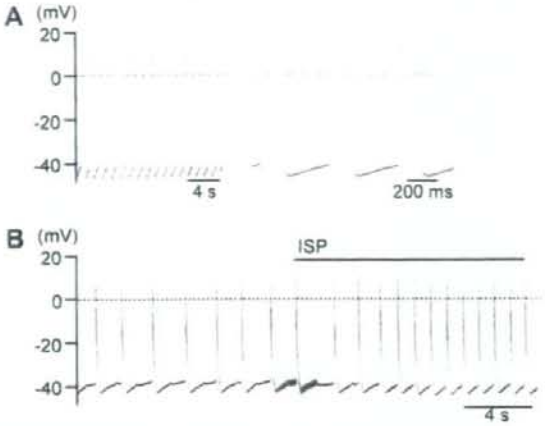

C

BCL (sec)	APD50 (msec)	APD90 (msec)
1.3~3.2	178.1±4.2	316.6±5.8

dV/dt max (V/s)	APA (mV)	MDP (mV)	n
5.6±1.0	68.4±2.5	-45.4±1.8	12

Fig. 3. Electrophysiology of CMESC-derived cardiomyocytes. (A) Representative action potentials of CMESC-derived cardiomyocytes showing spontaneous beating (left) and the relatively short duration time of the action potential (right). (B) Effect of isoproterenol (ISP) on the beating rate. (C) Statistical parameters obtained from 12 cardiomyocytes including beating cycle length (BCL), action potential duration (APD), d*V*/d*t* max, action potential amplitude (APA) and maximum diastolic potential (MDP).

Proliferative potential of CMESC-derived cardiomyocytes

Since the gestation period of the common marmoset is approximately seven times longer than that of the mouse, we hypothesized that CMESC-derived cardiomyocytes also retain their proliferative potential for a longer period of time and investigated this possibility. When EBs were dispersed into small clumps we observed a relatively long-term proliferation period and noticeable cell multiplication. From these findings, we expected that CMESC-derived cardiomyocytes might possess a higher proliferation ability than mouse-derived ES cells.

First, we performed BrdU incorporation assays on intact EBs at several time points after differentiation had occurred. The identification of DNA synthesizing cardiomyocytes was confirmed by co-immunofluorescent staining of Nkx2.5 and BrdU. At 6 weeks, intact EBs initially contained 33% BrdU-positive cardiomyocytes, but this decreased to less than 1% at 12 weeks (Fig. 4A and B). Next, the dispersed cells from EBs at several time points were applied to BrdU incorporation assays. Average 73% of cardiomyocytes were positive for BrdU at 5 weeks. This gradually decreased to 30% at 24 weeks, and 0% at 36 weeks (Fig. 4A and C). Most of the cardiomyocytes from freshly dispersed EBs 36 weeks after differentiation were rod-shaped (data not shown). These data indicated that common marmoset ES cell-derived cardiomyocytes retained their proliferation potential for an extended period of time.

Discussion

This is the first study to demonstrate that CMESC can differentiate into cardiomyocytes *in vitro*. We described their overall differentiation mechanism including time-courses for the expression of various genes during cardiogenesis, and characterized them in

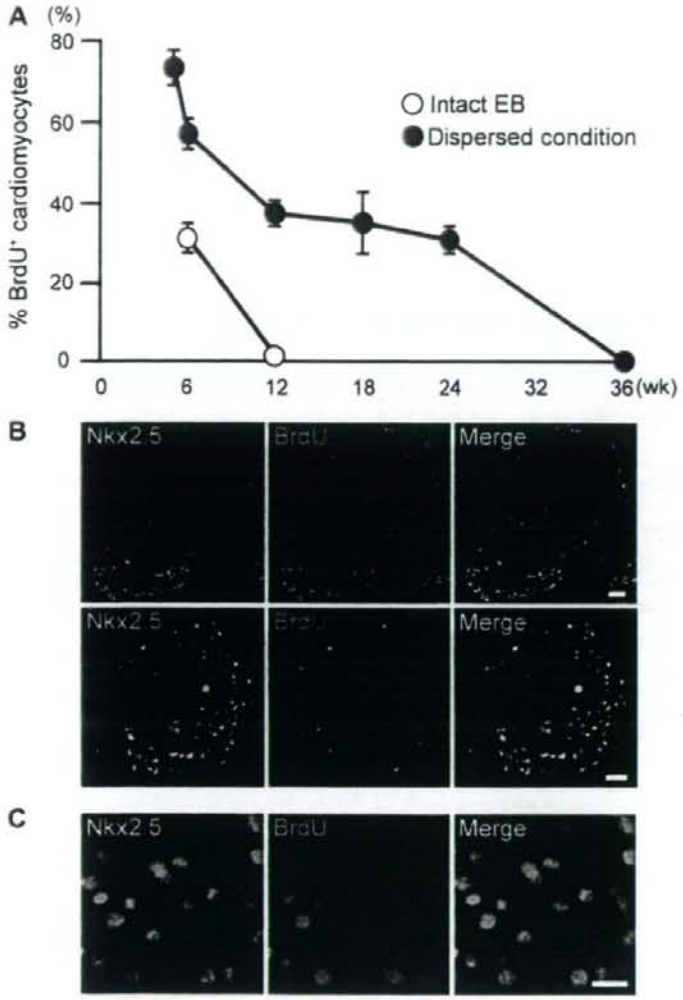

Fig. 4. Proliferation properties of CMESC-derived cardiomyocytes. (A) Time course BrdU incorporation assay in intact EB (open circle; $n = 3$) and dispersed condition (closed circle; $n = 3$) during weeks 5–36 post-differentiation. Cardiomyocytes were identified by immunofluorescent staining for Nkx2.5. The fractions of BrdU-positive cardiomyocytes were plotted. (B) Typical immunofluorescent staining patterns of Nkx2.5 (left), BrdU (middle) and merged images (right) in the intact EBs 6 weeks after differentiation (upper panel) and 12 weeks after differentiation (lower panel). (C) Typical immunodetection of Nkx2.5 (left), BrdU (middle) and merged images (right) in the dispersed condition 6 weeks after differentiation. Scale bars: (B) 100 μm; (C) 20 μm.

detail by immunofluorescent staining, ultrastructural analysis, electrophysiology and determining their growth properties.

Gene expression analyses during cardiogenesis in several species including mice [12], humans [13], and rhesus monkeys [10] are available. The present study enabled us to obtain gene expression data for the common marmoset monkey. A comparison of gene expression profiles between the species listed above highlights many similarities. The only major difference seems be in the timing of cardiomyocyte development: 8–14 days in humans; 12 days in the common marmoset; 8 days in the rhesus monkey; and 6 days in mice. Although minor differences in the expression timings of the *ANP*, *MLC-2a*, *MLC-2v* and *α-MHC* genes also exist during differentiation, we found that the timing of CMESCs was closest to human ES cells.

We found that the efficiency of cardiac differentiation was the same when obtained under non-serum conditions using KSR instead of FCS. These observations indicated that CMESCs, unlike human [14] or rhesus monkey [10] ES cells, do not require any serum-derived stimulating factors for mesendoderm induction and cardiogenesis, because KSR does not contain any cytokines or growth factors. On the other hand, the expression of various marker genes during cardiogenesis was very similar to that seen in human [14] and rhesus monkey [10] ES cells, suggesting that CMESCs have a similar cardiogenic differentiation system to human and rhesus monkey ES cells. CMESCs might be able to provide differentiation-inducing auto- and/or paracrine factors. Further mechanistic comparative studies between CMESCs and human and/or rhesus monkey ES cells will provide further insights into cardiogenic differentiation.

BrdU incorporation assay indicated that CMESC-derived cardiomyocytes were capable of long-term proliferation for extended periods of time. Importantly, CMESC-derived cardiomyocytes were still able to proliferate 24 weeks after differentiation, but the ability to proliferate ended at 36 weeks. Considering the gestation

period of the common marmoset, these findings had a reasonable explanation.

Much information about human ES cells and their application to heart regeneration therapy has accumulated [15,16]. Moreover, mouse and human inducible pluripotent stem cells (iPS cell) have also been established [17]. In order for heart regeneration therapy using regenerated cardiomyocytes to become a reality, preclinical studies using primate ES cell- or iPS cell-derived cardiomyocytes for transplantation are necessary. The common marmoset monkey is an ideal primate model for preclinical studies in the field of regenerative medicine. We believe that this report provides fundamental details about CMESC-derived cardiomyocytes that will aid their use as a primate heart cell-therapy model.

Appendix A. Supplementary data

Supplementary data associated with this article can be found, in the online version, at doi:10.1016/j.bbrc.2008.02.141.

References

[1] W.R. MacLellan, M.D. Schneider, Genetic dissection of cardiac growth control pathways, Annu. Rev. Physiol. 62 (2000) 289–319.
[2] B. Dawn, A.B. Stein, K. Urbanek, M. Rota, B. Whang, R. Rastaldo, D. Torella, X.L. Tang, A. Rezazadeh, J. Kajstura, A. Leri, G. Hunt, J. Varma, S.D. Prabhu, P. Anversa, R. Bolli, Cardiac stem cells delivered intravascularly traverse the vessel barrier, regenerate infarcted myocardium, and improve cardiac function, Proc. Natl. Acad. Sci. USA 102 (2005) 3766–3771.
[3] K.L. Laugwitz, A. Moretti, J. Lam, P. Gruber, Y. Chen, S. Woodard, L.Z. Lin, C.L. Cai, M.M. Lu, M. Reth, O. Platoshyn, J.X. Yuan, S. Evans, K.R. Chien, Postnatal isl1+ cardioblasts enter fully differentiated cardiomyocyte lineages, Nature 433 (2005) 647–653.
[4] H. Oh, S.B. Bradfute, T.D. Gallardo, T. Nakamura, V. Gaussin, Y. Mishina, J. Pocius, L.H. Michael, R.R. Behringer, D.J. Garry, M.L. Entman, M.D. Schneider, Cardiac progenitor cells from adult myocardium: homing, differentiation, and fusion after infarction, Proc. Natl. Acad. Sci. USA 100 (2003) 12313–12318.
[5] S. Lyngbaek, M. Schneider, J.L. Hansen, S.P. Sheikh, Cardiac regeneration by resident stem and progenitor cells in the adult heart, Basic Res. Cardiol. 102 (2007) 101–114.
[6] I. Kehat, D. Kenyagin-Karsenti, M. Snir, H. Segev, M. Amit, A. Gepstein, E. Livne, O. Binah, J. Itskovitz-Eldor, L. Gepstein, Human embryonic stem cells can differentiate into myocytes with structural and functional properties of cardiomyocytes, J. Clin. Invest. 108 (2001) 407–414.
[7] E. Sasaki, K. Hanazawa, R. Kurita, A. Akatsuka, T. Yoshizaki, H. Ishii, Y. Tanioka, Y. Ohnishi, H. Suemizu, A. Sugawara, N. Tamaoki, K. Izawa, Y. Nakazaki, H. Hamada, H. Suemori, S. Asano, N. Nakatsuji, H. Okano, K. Tani, Establishment of novel embryonic stem cell lines derived from the common marmoset (Callithrix jacchus), Stem Cells 23 (2005) 1304–1313.
[8] J.A. Thomson, J. Kalishman, T.G. Golos, M. Durning, C.P. Harris, R.A. Becker, J.P. Hearn, Isolation of a primate embryonic stem cell line, Proc. Natl. Acad. Sci. USA 92 (1995) 7844–7848.
[9] H. Suemori, T. Tada, R. Torii, Y. Hosoi, K. Kobayashi, H. Imahie, Y. Kondo, A. Iritani, N. Nakatsuji, Establishment of embryonic stem cell lines from cynomolgus monkey blastocysts produced by IVF or ICSI, Dev. Dyn. 222 (2001) 273–279.
[10] K. Schwanke, S. Wunderlich, M. Reppel, M.E. Winkler, M. Matzkies, S. Groos, J. Itskovitz-Eldor, A.R. Simon, J. Hescheler, A. Haverich, U. Martin, Generation and characterization of functional cardiomyocytes from rhesus monkey embryonic stem cells, Stem Cells 24 (2006) 1423–1432.
[11] M. Hosseinkhani, K. Hasegawa, K. Ono, T. Kawamura, T. Takaya, T. Morimoto, H. Wada, A. Shimatsu, S.G. Prat, H. Suemori, N. Nakatsuji, T. Kita, Trichostatin A induces myocardial differentiation of monkey ES cells, Biochem. Biophys. Res. Commun. 356 (2007) 386–391.
[12] K.R. Boheler, J. Czyz, D. Tweedie, H.T. Yang, S.V. Anisimov, A.M. Wobus, Differentiation of pluripotent embryonic stem cells into cardiomyocytes, Circ. Res. 91 (2002) 189–201.
[13] A. Beqqali, J. Kloots, D. Ward-van Oostwaard, C. Mummery, R. Passier, Genome-wide transcriptional profiling of human embryonic stem cells differentiating to cardiomyocytes, Stem Cells 24 (2006) 1956–1967.
[14] E. Bettiol, L. Sartiani, L. Chicha, K.H. Krause, E. Cerbai, M.E. Jaconi, Fetal bovine serum enables cardiac differentiation of human embryonic stem cells, Differentiation 75 (2007) 669–681.
[15] O. Caspi, I. Huber, I. Kehat, M. Habib, G. Arbel, A. Gepstein, L. Yankelson, D. Aronson, R. Beyar, L. Gepstein, Transplantation of human embryonic stem cell-derived cardiomyocytes improves myocardial performance in infarcted rat hearts, J. Am. Coll. Cardiol. 50 (2007) 1884–1893.
[16] M.A. Laflamme, K.Y. Chen, A.V. Naumova, V. Muskheli, J.A. Fugate, S.K. Dupras, H. Reinecke, C. Xu, M. Hassanipour, S. Police, C. O'Sullivan, L. Collins, Y. Chen, E. Minami, E.A. Gill, S. Ueno, C. Yuan, J. Gold, C.E. Murry, Cardiomyocytes derived from human embryonic stem cells in pro-survival factors enhance function of infarcted rat hearts, Nat. Biotechnol. 25 (2007) 1015–1024.
[17] K. Takahashi, S. Yamanaka, Induction of pluripotent stem cells from mouse embryonic and adult fibroblast cultures by defined factors, Cell 126 (2006) 663–676.